

## Response to Editor:

Thank you for submitting your manuscript entitled "Intensified Atlantic vs. weakened Pacific meridional overturning circulations in response to Tibetan Plateau uplift" [Paper #cp-2017-110] to *Climate of the Past*. I have now received an assessment of the two reviewers. Both reviewers had positive comments that require a minor revision prior to the publication of *Climate of the Past*.

Following reviewers concerns shall be addressed in the revised version to improve the quality of the manuscript:

1) Why does a removal of Tibetan Plateau leads to the intensified westerlies over the North Atlantic and weakened subtropical anticyclones and trade winds over the Pacific? Are these changes a direct atmospheric response of TP removal, or including feedbacks of SST?

In the last version of the manuscript (version-20180321-mark), we had addressed this issue accordingly, and at that time we had also replied as follows in our reply-to-reviewer file.

*First, the intensified westerlies over the North Atlantic in response to the TP removal is due to the absence of barrier effect from the TP allowing the atmospheric jet stream and associated low-level winds to become more zonal. Besides, the standing waves in association with the TP removal are also absent, leading to less orographic gravity wave drag and stronger winds (Palmer et al., 1986; Sinha et al., 2012). As shown in the revised version, the intensified surface westerly winds over the upstream of TP are clearly simulated (Fig. 2c on page 22).*

*Meanwhile, both theoretical studies and numerical simulations have demonstrated that the TP uplift strengthens the Asian summer monsoon and in turn diabatic heating over the Asian monsoon region, which provides a critical role in the formation and*

*maintenance of the summer North Pacific subtropical high (Ruddiman and Kutzbach, 1989; Rodwell and Hoskins, 2001; Kitoh, 2004). In particular, during the summertime, the upper-level divergence associated with strong monsoonal ascending motion is located over the Asian region and adjacent oceans, while the upper level convergence circulation related to the descending motion is observed over the middle and lower latitudes of eastern Pacific (Please see the following Fig. S1a). Comparatively, this circulation cell in the NTP is not as strong as in the MTP, indicating the weakening of both the North Pacific subtropical high and Asian monsoon (Please see the following Figs. S1b and S1c).*

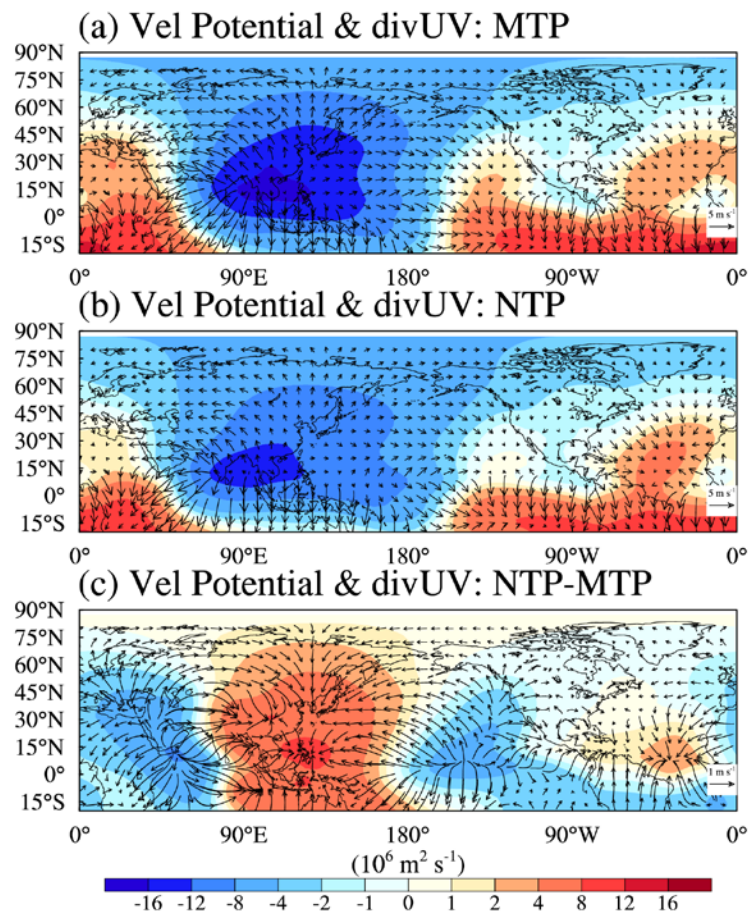


*Figure S1. The Northern Hemisphere summertime mean velocity potential (contour) and divergent wind (vectors) at 200 hPa for the (a) MTP, (b) NTP, and (c) the differences between NTP and MTP.*

*Second, following your comment, we have supplemented a set of experiments with and without TP undertaken by the atmospheric general circulation model (AGCM) of CESM version 1.0.5, aiming to examine the feedback originating from the sea surface temperature changes. The 200-year climatologically averaged sea surface temperature prescribed in both the AGCM experiments is obtained from the MTP experiments undertaken by coupled atmosphere–ocean general circulation model (CGCM, CESM version 1.0.5). Both AGCM experiments are integrated for 50 model years, and the further analysis is performed based on the results of the last 30-year simulations.*

*In the CGCM experiments, the removal of the TP significantly causes a weakening of the North Pacific subtropical high and an overall weakening of the low-level tropical trade winds (Please see the following Fig. S2a). Similar changes are seen in the AGCM experiments, but with an overall weaker intensity (Please see the following Fig. S2b). Relative to the results of AGCM experiments, there is a clear decrease of tropical trade winds over the North Pacific and an increase of low-level westerly over the North Atlantic in the CGCM experiments (Please see the following Fig. S2c), indicating that the changes of sea surface temperature and oceanic circulations further amplify atmospheric circulation anomalies due to the TP uplift. Thus, we believe that the decrease of AMOC in our simulations is primarily attributed to the direct response of atmospheric circulation to the removal of the TP, and the oceanic feedback further amplifies this response. Considering the aforementioned atmospheric responses in association with the TP uplift have been addressed by many AGCM and CGCM simulations, we do not describe them in detail. Alternatively, we have added a short description on these processes in the revised version (L149–154).*

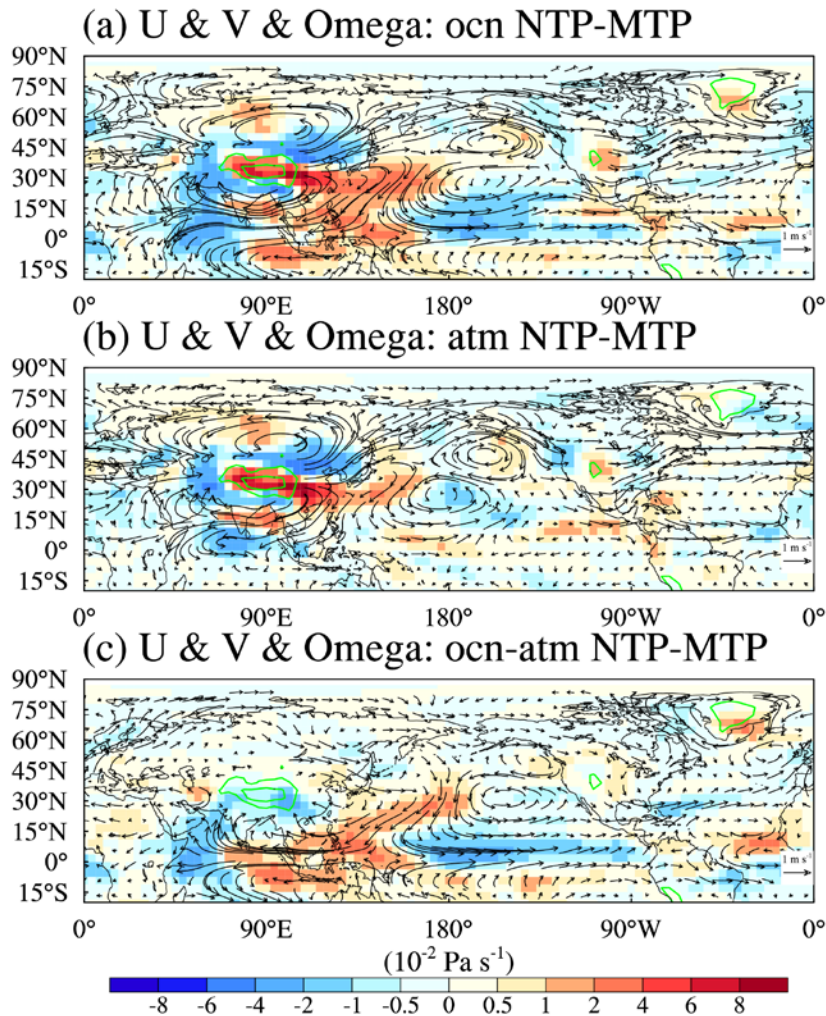


Figure S2. Changes of annual mean 500 hPa vertical velocity and 850 hPa wind in NTP relative to MTP for the (a) CGCM, (b) AGCM, and (c) differences between CGCM and AGCM. Green contours surround the areas with topography higher than 2000 m and 4000 m, respectively.

For details, please refer to L149–156 in the current version of the manuscript.

2) In the NTP experiment, the net freshwater flux increases by 0.005 Sv at the initial stage, but by 0.025 Sv at the final stage. The author should discuss if fresh water flux of 0.005Sv is strong enough to trigger the weakening of AMOC.

In the last version of the manuscript (version-20180321-mark), we had addressed this issue accordingly, and at that time we had also replied as follows in our reply-to-reviewer file.

*We have compared the magnitude of net freshwater flux in our simulations with two earlier simulations, although there exists difference in the experimental configuration. Sinha et al. (2012) indicated a final net precipitation flux anomaly of approximately 0.02 Sv across the Atlantic basin (30–60°N). Maffre et al. (2017) indicated that the net freshwater flux anomaly over the North Atlantic (22–60°N) is approximately 0.0446 Sv and 0.097 Sv at the beginning and final stages, respectively. First, it should be noted that these two previous simulations with respect to the freshwater flux anomaly are obtained from simulations with and without global mountains, rather than the TP alone in our experiments. As such, the atmospheric circulation responses to the topographic modification in their experiments might be stronger than ours. Second, the area that they calculated the freshwater flux is over the North Atlantic at 22–60°N, and the grid mesh is greater in size than ours at 40–70°N. Third, Maffre et al. (2017) emphasized the net freshwater flux over the tropical Atlantic could play an important role in the AMOC weakening. We do not exclude the importance of the net freshwater flux over the tropical–subtropical Atlantic, since it has been well revealed that the warm and salty waters of the tropical–subtropical North Atlantic circulate north to the sub-polar regions of the North Atlantic via the Gulf Stream, and evaporation causes the surface waters to cool and thus the formation of North Atlantic Deep Water. Even though the net freshwater flux in our simulations is less than that in Maffre et al. (2017), it is difficult for us to determine the sensitivity of AMOC in response to the net freshwater flux in our simulations. Because we have identified the important role of wind-driven sea-ice process in initially triggering the AMOC weakening in our simulations. Thus, to answer the abovementioned question, a series of sensitivity experiments with the modification of*

*the net freshwater flux are necessary to be performed. However, this topic is beyond the scope of this study and needs to be investigated in the future.*

Furthermore, we have added a preliminary comparison with recent simulations with and without global mountains in the current version (L169–174): “It should be noted that these changes in freshwater budget in our simulations are less than approximately 0.0446 Sv and 0.097 Sv of recent simulations with and without global mountains (Maffre et al., 2017), and the time for a complete collapse the AMOC in our NTP simulation (Figure 3b) is also longer (approximately 700 years) than for their experiments without global mountains (approximately 400 years). Such a difference should be related to the experimental design and the sensitivity of the models to freshwater forcing.”.

3) The T31 version of CESM is known to have significant climate biases, especially in high-latitude regions that are a main focus for this paper (including Arctic sea ice extent). Implications of these model biases on the results and conclusions shall be discussed.

In the last version of the manuscript (version-20180321-mark), we had addressed this issue accordingly, and at that time we had also replied as follows in our reply-to-reviewer file.

*We agree that the low resolution version of CESM has a cold bias against the observation, especially in the North Atlantic high latitudes, which is partly attributed to the deficit of ocean heat transport and the excess of Arctic sea-ice (Shields et al., 2012). More specifically, in the pre-industrial simulation (MTP), there is a weak positive slope in the long-term global mean temperature, in particular at the beginning of simulations; and global mean temperature reaches a quasi-equilibrium state at approximately 12 °C,*

*which is lower than observations (please see Fig. 1c on page 21). In the revised version, we have mentioned this model bias and its potential influence on the simulations (L257–259).*

For details on the model bias and its implications, please refer to L263–266 in the current version of the manuscript.

4) Avoid use of "vs." in the title and replace it with the word "difference" e.g. "Difference between the Atlantic and Pacific meridional overturning circulation in response to the uplift of the Tibetan Plateau"

The suggested title has been taken in the revised version. Thanks a lot!

The current marked-up manuscript version relative to the version-20180321:

1        ~~**Intensified Atlantic vs. weakened Pacific meridional overturning**~~  
2        ~~**circulations in response to Tibetan Plateau uplift**~~ **Difference between**  
3        **the North Atlantic and Pacific meridional overturning circulation in**  
4        **response to the uplift of the Tibetan Plateau**

5        Baohuang Su<sup>1,4</sup>, Dabang Jiang<sup>1,2,3,4</sup>, Ran Zhang<sup>1</sup>, Pierre Sepulchre<sup>5</sup>, and Gilles Ramstein<sup>5</sup>

6        <sup>1</sup>Institute of Atmospheric Physics, Chinese Academy of Sciences, Beijing 100029, China

7        <sup>2</sup>Joint Laboratory for Climate and Environmental Change at Chengdu University of Information Technology,  
8        Chengdu 610225, China

9        <sup>3</sup>CAS Center for Excellence in Tibetan Plateau Earth Sciences, Beijing 100101, China

10       <sup>4</sup>University of Chinese Academy of Sciences, Beijing 100049, China

11       <sup>5</sup>Laboratoire des Sciences du Climat et de l'Environnement/IPSL, CEA-CNRS-UVSQ, UMR8212, Orme des  
12       Merisiers, CE Saclay, 91191 Gif-sur-Yvette Cedex, France

13       **Abstract:** The role of the Tibetan Plateau (TP) in maintaining the large-scale overturning  
14       circulation in the Atlantic and Pacific is investigated using a coupled atmosphere–ocean model. For  
15       the present day with a realistic topography, model simulation shows a strong Atlantic meridional  
16       overturning circulation (AMOC) but a near absence of the Pacific meridional overturning  
17       circulation (PMOC), which are in good agreement with the present observations. In contrast, the  
18       simulation without the TP depicts a collapsed AMOC and a strong PMOC that dominates deep  
19       water formation. The switch in deep water formation between the two basins results from changes  
20       in the large-scale atmospheric circulation and atmosphere–ocean feedback over the Atlantic and  
21       Pacific. The intensified westerly winds and increased freshwater flux over the North Atlantic cause  
22       an initial slowdown of the AMOC, while the weakened East Asian monsoon circulation and  
23       associated decreased freshwater flux over the North Pacific give rise to the initial intensification of

24 the PMOC. The further decreased heat flux and the associated increase in sea-ice fraction promote  
25 the final AMOC collapse over the Atlantic, while the further increased heat flux leads to the final  
26 PMOC establishment over the Pacific. Although the simulations were done in a cold world, it still  
27 importantly implicates that the uplift of the TP alone could have been a potential driver for the  
28 reorganization of PMOC–AMOC between the Late Eocene and Early Oligocene.

## 29 1. Introduction

30 The uplift of the Tibetan Plateau (TP) was a major tectonic event that had occurred throughout  
31 the Cenozoic, and its gradual growth had exerted a strong influence on the atmospheric circulation  
32 and climate (Molnar et al., 2010). Since the pioneering work of Bolin (1950), the impacts of  
33 mountain uplift on regional and global climate have been extensively investigated. Nevertheless,  
34 most studies have emphasized the role of mountain ranges on atmosphere dynamics, while  
35 quantifications of the associated impact on ocean dynamics have been rare. For example, most  
36 previous works have taken atmospheric general circulation models to address regional climate  
37 effects, notably the Asian monsoon and arid environment evolutions (e.g., Ruddiman and Kutzbach,  
38 1989; Ramstein et al., 1997; An et al., 2001; Liu and Yin, 2002; Jiang et al., 2008; Zhang et al.,  
39 2015). However, simulations have recently been applied to investigate the effect of mountain uplift  
40 in the context of the atmosphere–ocean system, and a few studies have proposed that the uplift of  
41 the Andes (Sepulchre et al., 2009) and Rocky Mountains (Seager et al., 2002) is closely linked to  
42 the evolution of oceanic circulations, including the Gulf Stream and Humboldt Current, and the El  
43 Niño–Southern Oscillation system (Feng and Poulsen, 2014). Although it has been indicated that  
44 the TP uplift affects sea surface temperatures, sea surface salinity, precipitation, and trade winds for  
45 both the Pacific and equatorial Indian Ocean (Abe et al., 2003; Kitoh, 2004; Okajima and Xie,  
46 2007), the influence of the TP uplift on the high-latitude oceanic circulations, particularly in the  
47 North Atlantic, has rarely been explored.

48 The potential importance of mountain uplift in modifying the oceanic thermohaline circulation

49 has previously been investigated. Ruddiman and Kutzbach (1989) indicated that mountain  
50 uplift-induced changes in the North Atlantic surface circulation are expected to increase the North  
51 Atlantic Deep Water formation. In addition, Rind et al. (1997) performed the coupled model  
52 simulations with and without TP and proposed that the TP may have a considerable impact on the  
53 large-scale meridional overturning circulation (MOC). However, the integration time used in this  
54 pioneering simulations was too short to fully evaluate the deep oceanic circulation response, and  
55 thus more studies are still needed to evaluate the possible role of the TP in modulating the MOC.

56 On a geological timescale, remarkable reorganization and evolution of the large-scale oceanic  
57 overturning circulation, from the Southern Ocean deep water dominating mode to the modern-like  
58 North Atlantic deep water mode, have been evidenced through the Late Eocene to the Early  
59 Oligocene (Wright and Miller, 1993; Davies et al., 2001; Via and Thomas, 2006). This dramatic  
60 shift is possibly associated with major rearrangements in the ocean seaways and other tectonic  
61 changes, although the ultimate trigger is still being debated (Zhang et al., 2011). In addition, it is  
62 suggested that the regional surface of the TP had reached a high elevation of more than 4000 meters  
63 around 40 Ma ago (Dupont-Nivet et al., 2008; Wang et al., 2008), although debates regarding  
64 paleoaltitude reconstructions remain (Botsyun et al., 2016). Given this timing of TP uplift, it is  
65 important to quantify the contribution of TP uplift on the meridional oceanic circulation of the  
66 Northern Hemisphere. In this study, therefore, two coupled atmosphere–ocean numerical  
67 integrations, with and without TP, are designed to investigate the role of the TP on the Atlantic  
68 MOC (AMOC) and Pacific MOC (PMOC).

## 69 2. Model, experimental design, and density flux analysis

### 70 2.1. Model and experiments

71 The Community Earth System Model (CESM) version 1.0.5 of the National Center for  
72 Atmospheric Research is a widely used, well-validated coupled model with dynamic atmosphere,  
73 land, ocean, and sea-ice components (Gent et al., 2011). It is applied to this study at a

74 low-resolution configuration that is computationally efficient and well-described (Shields et al.,  
75 2012) and employs an atmospheric horizontal grid of roughly  $3.75^\circ \times 3.75^\circ$  (T31) with 26 vertical  
76 levels. The ocean model adopts a finer oceanic horizontal grid, with a nominal  $3^\circ$  resolution  
77 increasing to  $1^\circ$  near the equator ( $116 \times 100$  grid points, latitude by longitude) and 60 unevenly  
78 spaced layers in the vertical direction. The sea-ice and land models share the same horizontal grids  
79 as the ocean and atmosphere models, respectively, where the sea-ice component is a  
80 dynamic–thermodynamic model that includes a subgrid-scale ice thickness distribution and  
81 energy-conserving thermodynamics (Holland et al., 2012).

82 Two experiments are conducted; firstly, a control run with the modern topography (MTP,  
83 Figure 1a), and secondly a sensitivity run where topography within the region of  $20\text{--}60^\circ\text{N}$  and  
84  $60\text{--}140^\circ\text{E}$  at altitudes higher than 200 m is set to 200 m (NTP, Figure 1b), which enables  
85 examination of the climate effect in relation to the TP topography. This TP uplift configuration has  
86 been referred to in the majority of previous simulation works (e.g., Liu and Yin, 2002; Jiang et al.,  
87 2008). This greatly simplified topographic setting is not intended to represent a realistic scenario  
88 constrained by the geological evidence and instead represents two end-members of the potential  
89 growth histories of the TP. So, it is important to note that these experiments only aim to investigate  
90 the TP uplift occurring in “a cold world” with an atmospheric  $\text{CO}_2$  corresponding to the  
91 pre-industrial values (284.0 ppm). With the exception of topography, all the other boundaries, such  
92 as land–sea distribution and orbital parameters, are prescribed to pre-industrial conditions. The MTP  
93 is continually integrated for 1100 years, and the NTP is additionally integrated for another 1840  
94 years starting from the year 1100 of the MTP. Global mean surface air temperature and sea  
95 temperature at a depth of 1000 m are shown in Figure 1c. Both simulations reach equilibrium states  
96 after more than 1000 model years of integration time, and the final 200 years of both cases are  
97 applied for our climate state analysis.

## 98 2.2. Density flux analysis

99 Because one of the major aims of this paper is to analyze changes in the meridional oceanic  
 100 circulation, we decided to focus on the density flux parameter, which is appropriate to diagnose  
 101 these oceanic circulation changes. The dense deep water masses are formed in the area with  
 102 relatively high surface density achieved by cooling or increasing salinity. To better understand  
 103 which processes dominated the MOC changes in simulations, it is instructive to further analyze the  
 104 time evolution of density fluxes budget. Therefore, a density flux analysis method, in which the  
 105 total density flux decomposes into the haline contribution due to freshwater flux and the thermal  
 106 contribution due to heat flux (Schmitt et al., 1989), is adopted in our study. The total density flux is  
 107 calculated from a linearized state equation of seawater, as

$$F_{\rho} = -\alpha \cdot \frac{Q}{C_p} + \rho(0, T) \cdot \beta \cdot \frac{(E - P - R - I) \cdot S}{1 - S}$$

108  $F_{\rho}$  is the total density flux,  $-\alpha \cdot \frac{Q}{C_p}$  is thermal density flux, and  $\rho(0, T) \cdot \beta \cdot \frac{(E - P - R - I) \cdot S}{1 - S}$  is haline  
 109 density term.  $C_p$ ,  $T$ , and  $S$  are the specific heat capacity, surface temperature and salinity of  
 110 seawater, respectively.  $\alpha$  and  $\beta$  are the thermal expansion and haline contraction coefficients,  
 111 respectively.  $\rho(0, T)$  is the density of freshwater with a salinity of 0 psu and temperature of  $T$ .  $Q$   
 112 represents the net surface heat flux.  $E$ ,  $P$ ,  $R$ , and  $I$  denote the freshwater fluxes due to  
 113 evaporation, precipitation, river runoff, and sea-ice melting (or brine rejection), respectively.

### 114 3. Results

#### 115 3.1. Changes in AMOC and PMOC

116 There are evident changes in the AMOC and PMOC indices in response to the TP uplift  
 117 (Figure 1d). With MTP, the AMOC stabilizes at around 17 Sv ( $\text{Sv} = 10^6 \text{ m}^3 \text{ s}^{-1}$ ) for more than 1000  
 118 years (Figure 1d, 1–1100 years, red line), which agrees with the observations  $18.7 \pm 5.6$  Sv for  
 119 2004–2005 (Cunningham et al., 2007), but with NTP there is a continual weakening of the AMOC  
 120 until the point of quasi-collapse (ca. 2 Sv, Figure 1d). In contrast, the PMOC of NTP begins at a  
 121 sluggish level from MTP (Figure 1d, 1–1100 years, purple line) and takes as long as 1200 years to

122 reach an equilibrium state that is comparable to the level of the AMOC in MTP (ca. 18 Sv, Figure  
123 1d, 1101–2940 years, purple line). In agreement with the dramatic responses of AMOC and PMOC,  
124 sea surface salinity increases in the North Pacific but decreases in a broad area of the North Atlantic  
125 (Figure 2b). To fully understand the different behaviors between AMOC and PMOC in NTP, in the  
126 following sections we further analyze changes in the atmospheric and oceanic circulations and the  
127 atmosphere–ocean feedbacks.

### 128 3.2. Atmospheric responses

129 The modified AMOC and PMOC are linked to the large-scale atmospheric circulation changes.  
130 In terms of model results of the NTP relative to the MTP, the surface air temperature over and  
131 around the TP and in the North Pacific increased but decreased over the North Atlantic (Figure 2a),  
132 which agrees with the previous simulations (Broccoli and Manabe, 1992; Kutzbach et al., 1993). In  
133 addition, there are intensified westerlies over the North Atlantic and weakened subtropical  
134 anticyclones and trade winds over the North Pacific (Figure 2c); the former results from a  
135 significant increase in the meridional pressure gradient driven by a large-scale equatorward shift of  
136 air mass occupying the current position of the TP (Figure 2c) and from a reduced drag of the  
137 orographically induced gravity waves associated with the absence of the TP (Palmer et al., 1986;  
138 Sinha et al., 2012), while the latter is derived from the weakening of zonal Eurasia–Pacific thermal  
139 contrast in the middle troposphere (not shown), especially in boreal summertime, in relation to  
140 removal of the mountains (Ruddiman and Kutzbach, 1989; Rodwell and Hoskins, 2001; Kitoh,  
141 2004).

142 When the TP is removed, the atmospheric moisture transport between the Pacific and Atlantic  
143 Oceans undergoes a basin-basin asymmetric redistribution as a response to the large-scale  
144 circulation anomalies (Figure 2c). In comparison with MTP results, the NTP simulation shows large  
145 amounts of anomalous westerly moisture flux transported through the lowlands of Central America  
146 to the North Atlantic, causing weak moisture convergence therein (Figure 2d). In addition, removal

147 of the TP leads to a significant divergence of moisture over East Asia and the western North Pacific  
148 marginal seas (Figure 2d), which is linked to a weakened monsoon circulation and is consistent with  
149 the previous simulations using both atmospheric and coupled ocean–atmosphere general circulation  
150 models (Liu and Yin, 2002; Kitoh, 2004; Molnar et al., 2010). The anomalies of atmospheric  
151 circulation shown above are derived partially from the positive feedback caused by the changed sea  
152 surface temperature due to the removal of the TP. In particular, the weakening of both the Asian  
153 monsoon and North Pacific subtropical anticyclone in association with the TP removal ~~were~~are  
154 shown to be greater in the context of coupled model as compared to that in atmosphere-only model  
155 due to the additional ocean–atmosphere feedback (Kitoh, 2004). Thus, the atmosphere–ocean  
156 feedbacks also play an important role in maintaining the inter-basin atmospheric moisture  
157 asymmetric redistribution.

### 158 3.3. Oceanic responses and atmosphere–ocean feedbacks

#### 159 3.3.1. Changes in freshwater and sea-ice

160 The above changes in the large-scale atmospheric circulation markedly decrease the total  
161 ocean density flux in the North Atlantic (Figure 3a, brown), supporting the trend of the AMOC  
162 (Figure 1d). Both the increases of net freshwater and wind-driven sea-ice expansion are responsible  
163 for the initial reduction of total ocean density flux and further induce a gradual weakening of the  
164 AMOC. In more details, on the one hand, the anomalous atmospheric circulation associated with  
165 the removal of the TP ~~transports~~drives more water vapor ~~transportation~~ northward (Figure 2d)  
166 over the North Atlantic Ocean, causing more precipitation at the beginning of NTP simulation  
167 (Figure 3b, ca. 1101–1200 years, red line). Correspondingly, the net freshwater flux (precipitation  
168 plus runoff minus evaporation) convergence into the North Atlantic basin at 40°–70°N increases by  
169 0.005 Sv (~3%) and 0.025 Sv (~16%) at the initial and final states of NTP simulations (Figure 3b,  
170 green), respectively. It should be noted that these changes in freshwater budget in our simulations  
171 are less than approximately 0.0446 Sv and 0.097 Sv of recent simulations with and without global

172 mountains (Maffre et al., 2017), and the time for a complete collapse of the AMOC in our NTP  
173 simulation (Figure 3b) is also longer (approximately 700 years) than for their experiments without  
174 global mountains (approximately 400 years). Such a difference should be related to the  
175 experimental design and the sensitivity of the models to freshwater forcing.

176 ~~Moreover,~~ There is also a significant increase in the area-averaged sea-ice coverage over the  
177 North Atlantic through wind-driven processes (Figure 3c, green). With the TP, the annual mean  
178 sea-ice forms mainly in the northern and western region of the sub-polar North Atlantic, and it shifts  
179 southward and eastward when driven by cyclonic wind stress associated with the Icelandic Low,  
180 and melts in the Labrador Sea (sub-polar gyre) caused by a warm condition (Figure 4a). By  
181 comparison, after removal of the TP, anomalously intensified cyclonic winds induce an anomalous  
182 eastward sea-ice velocity (Figure 4c), and ~~cause~~ also a rapid eastward shift of the sea-ice margin  
183 (Figure 4c). Meanwhile, the locally melted sea-ice due to thermodynamics processes reduces in the  
184 southeast of Greenland (red shading, Fig. 4c), but increases in the south of Greenland (blue shading,  
185 Fig. 4c). It suggests that there is more sea-ice transporting from the high latitudes into the sub-polar  
186 gyre region, and the anomalous expansion of sea-ice margin in this region primarily originates from  
187 the wind-driven eastward transportation (dynamics processes), but not the local formation  
188 (thermodynamic processes). Because of this increased sea-ice through thermodynamically  
189 insulating the sea water from the freezing air, the release of sensible and latent heat into the  
190 atmosphere decreases and the density of sea water finally reduces, which processes have also been  
191 previously elucidated by Zhu et al. (2014).

192 Moreover, the total ocean density flux increases in the North Pacific in response to the removal  
193 of the TP. Due to the weakened Asian monsoon circulation and associated decrease in rainfall and  
194 runoff after lowering the topography, the net freshwater flux received by the North Pacific decreases  
195 by 0.08 Sv (~26%) and 0.12 Sv (~40%) during the initial and end stages of the NTP simulation,  
196 respectively (Figure 6b, green). This continuous negative freshwater flux forcing tends to increase  
197 density and initially leads to the formation of the North Pacific dense water, which is verified from

198 changes in the haline density flux (Figure 6a). Specifically, during the first 200 years of the NTP run,  
199 the haline density flux constantly produces a net positive contribution to the total density relative to  
200 the MTP haline term (Figure 6a, blue line). Meanwhile, the thermal density flux remains at a lower  
201 level (Figure 6a, ca. 1101–1300 years, red line) relative to the MTP. Thus, it indicates that the  
202 initially increased density of the North Pacific is largely attributed to the haline density term, but  
203 not the thermal density term.

### 204 3.3.2. Roles of the atmosphere–ocean feedbacks

205 The aforementioned weakening of the AMOC due to the atmospheric processes further triggers  
206 a positive atmosphere–ocean feedback loop through reducing northward heat transport, and  
207 subsequent decreasing sea surface temperatures, then allowing sea-ice to expand, suppressing the  
208 release of evaporating latent and sensible heat, and reducing the sea water density, and further  
209 weakening the AMOC, as previously shown in Jayne and Marotzke (1999) and Zhu et al. (2014).

210 Note that the negative effect of net freshwater becomes increasingly unimportant in  
211 comparisoneompared to the heat flux feedback associated with the latent/sensible heat changes  
212 (Figure 3a). Finally, the thermal density flux decreases by 49% relative to the MTP run, which  
213 substantially dominates the total density flux changes (Figure 3a). To be specific, the annual mean  
214 total density flux and mixed layer depth over the North Atlantic, especially around the Iceland  
215 where the collapse of deep water formation occurs, is dramatically decreased in NTP (Figure 5d, the  
216 maximum mixed layer depth is approximately 100 m) in comparison to that in MTP (Figure 5a, the  
217 maximum mixed layer depth is approximately 900 m). Moreover, this reduced total density flux  
218 over the North Atlantic is more attributed to the decreased thermal density flux associated with less  
219 latent and sensible release (Figure 5e) than the changed haline density flux (Figure 5f).

220 Atmosphere–ocean feedbacks also strengthen the PMOC. Due to the initial development of the  
221 PMOC mentioned in section 3.1, a positive feedback (as pointed out in Warren (1983)) is initiated  
222 by the intensifying meridional oceanic circulation; -, which this transports warmer subtropical water

223 northward and leads to the buoyancy loss and evaporation increase (Figure 6b). This feedback is  
224 also able to re-trigger PMOC enhancement. By comparison to the changes in the North Atlantic,  
225 both the regionally averaged sea-ice coverage (Figure 6c) and February sea-ice margin (Figure 4f)  
226 over the North Pacific experience a slightly northward retreat and have a relatively smaller effect on  
227 the simulated strengthening of the PMOC. Over a longer time, the thermal density flux, which is  
228 due to the loss of total heat, contributes more to the total density flux than the haline flux in relation  
229 to reduction in the net freshwater discharge (Figure 6b). Spatially, both increased total density flux  
230 and mixed layer depth in the North Pacific Ocean show opposite change characteristics with the  
231 North Atlantic (Figure 7d). Correspondingly, in comparison to the MTP, there is a widespread  
232 increase of the thermally induced density flux in the sub-polar North Pacific in NTP (Figure 7f), but  
233 with little spatially changed in the haline density flux (Figure 7f). Thus, in contrast to the results  
234 shown in the North Atlantic, the increased total heat exchange between the atmosphere and ocean  
235 due to the processes of sensible and latent heat releases (Figure 6b) ultimately becomes a dominant  
236 factor in maintaining a vigorous PMOC by controlling the increased total density flux (Figure 6a).

#### 237 4. Conclusions and Discussion

238 This study investigates the effect of TP uplift on the large-scale oceanic circulation using a  
239 low-resolution version of CESM. Results show that the removal of the TP initially changes the  
240 wind-driven atmospheric moisture transport process and the wind-driven sea-ice coverage  
241 expansion process, which are responsible for the initial weakening of the AMOC. Meanwhile, the  
242 suppressed monsoonal circulation in East Asia and the western Pacific marginal seas induces the  
243 decrease of rainfall and runoff and further causes the initially increased PMOC. Moreover, the  
244 positive feedback further changes the AMOC and PMOC. In particular, the AMOC weakening can  
245 further decrease the North Atlantic sea surface temperatures, ocean–atmosphere temperature  
246 contrast, evaporation, and precipitation, and subsequently increase sea-ice coverage. These  
247 processes together cause the final changes of the AMOC and PMOC (Figure 8).

248 A previous study demonstrated the role of Rocky Mountain uplift on heat transport and Gulf  
249 Stream patterns in the North Atlantic (Seager et al., 2002). In this study, we focus on the most  
250 prominent long-term orogenesis occurring since the Eocene: the TP and Himalayan uplift and  
251 associated impacts on the MOC. Our results can be compared with those derived from the earlier  
252 simulations, although experimental configurations differ somewhat. It has been indicated that the  
253 removal of global mountains triggers the collapse of deep water in the North Atlantic but enables  
254 formation in the North Pacific in three different coupled models (Schmittner et al., 2011; Sinha et  
255 al., 2012; Maffre et al., 2017). The simulated weakening of the AMOC is also qualitatively  
256 consistent with recent experiments using a decreased elevation of the TP and Central Asia (Fallah et  
257 al., 2016). However, only TP topography is reduced in our study, but our results are comparable  
258 with those of the ~~earlier~~past studies, therefore highlighting the key role that TP has played in  
259 forming the current large-scale deep oceanic circulation pattern. Nevertheless, given that all existing  
260 simulations (including ours) have used a rather coarse resolution of the coupled model  
261 configuration, it is considered that a finer resolution model may provide a better representation of  
262 the western boundary currents and allow for a more accurate and realistic resolving of the ocean  
263 eddies, which are believed to be critically important oceanic processes that should be taken in the  
264 realistic simulations of the AMOC (Spence et al., 2008). In addition, the low-resolution CESM is  
265 also found to generally have a cold bias with the underestimated ocean heat transport and excessive  
266 Arctic sea-ice (Shields et al., 2012), which could potentially exert modulations on the AMOC  
267 weakening. It is thus considered that investigating the response of the PMOC and AMOC to the TP  
268 uplift using an atmosphere–ocean general circulation model with a higher spatial resolution would  
269 be useful. Besides, the robust changes in the AMOC and PMOC, and the associated mechanisms  
270 due to the TP uplift can be evaluated through multi-model comparison.

271 Based on a comprehensive analysis of modern climatological data, Warren (1983) and  
272 Emile-Geay et al. (2003) hypothesized that the present MOC (mainly occurring in the Atlantic but  
273 not in the Pacific) is determined by the large mountains, namely the Himalayas and Rockies, which

274 induce an asymmetric distribution of wind stress and moisture transport features between the  
275 Atlantic and Pacific basins. However, previous studies have also demonstrated that the asymmetric  
276 continental extents and basin widths (basin geometries) between the two basins (Weaver et al., 1999;  
277 Nilsson et al., 2013) also play a possible key role in maintaining the present day AMOC. Our  
278 simulations support the hypothesis proposed by Warren (1983) and highlight the significant role of  
279 the TP alone in maintaining the modern AMOC. Moreover, the similar PMOC–AMOC seesaw  
280 dynamics have also been seen in simulations (Saenko et al., 2004; Chikamoto et al., 2012; Hu et al.,  
281 2012) as well as in reconstructions (Okazaki et al., 2010; Menviel et al., 2014; Freeman et al., 2015)  
282 for the last deglaciation. Such studies have also suggested that large PMOC–AMOC seesaw  
283 modulations can be triggered by slight changes in the freshwater/salinity redistributions between the  
284 Pacific and Atlantic. Furthermore, we provide an insight that the maintenance mechanism of PMOC  
285 in [the simulation](#) without the TP, to some extent, is the same as the AMOC in the present day.  
286 Specially, for the current North Atlantic, there is a persistently northward movement of warm and  
287 salty water mass from the tropical-subtropical Gulf Stream region into North Atlantic and farther  
288 poleward into the Norwegian and Greenland Seas, where it is exposed to very cold atmospheric  
289 temperatures and followed by a gradual cooling and in turn a higher density due to the release  
290 substantial sensible and latent heat into the overlying cold atmosphere, which is the same as PMOC,  
291 before eventually forming the North Atlantic Deep Water.

292 Our simulations have potential implications for understanding paleotemperature reconstructions  
293 and paleoceanographic circulation reorganization. The Earth has experienced a long-term cooling  
294 trend throughout the Cenozoic as testified by many proxies and stacked records (Zachos et al., 2001,  
295 2008), in association with an increased equator-to-pole thermal gradient. A very important  
296 contribution to understanding the large cooling during the Cenozoic has been determined as the  
297 drastic decrease in atmospheric CO<sub>2</sub> since the Eocene (DeConto and Pollard, 2003; DeConto et al.,  
298 2008). On the other hand, a study with new data base further indicated that this thermal evolution  
299 has been different among ocean basins during the Cenozoic (Cramer et al., 2009), and this differing

300 evolutionary pattern between basins is largely related to the large-scale ocean dynamics and tectonic  
301 events (Zhang et al., 2011). Moreover, epsilon-Neodymium (eps-Nd) isotopes in the deep Pacific  
302 suggest that the North Pacific was characterized by vigorous deep water formation during ca. 65–40  
303 Ma (Thomas, 2004). Other new eps-Nd records also confirm that the overturning circulation was  
304 already established in the high-latitude North Pacific prior to 40 Ma (Hague et al., 2012; Thomas et  
305 al., 2014). ~~Comparatively~~In comparison, a modern-like bipolar oceanic circulation, characterized by  
306 two branches of deep water formation in the Southern Ocean and the North Atlantic, began in the  
307 late Eocene (~38.5 Ma) in relation to the effect of Southern Ocean gateway openings (Borrelli et al.,  
308 2014). Several records also support that the onset of the present AMOC state began at the  
309 Eocene–Oligocene transition (~34 Ma) in association with the tectonic deepening of the  
310 Greenland–Norwegian Sea (Wright and Miller, 1993; Davies et al., 2001; Via and Thomas, 2006).  
311 However, it is likely that the intermittent Cenozoic uplift of the TP reached a certain height by the  
312 Early Oligocene, as shown in geologic evidences (Dupont-Nivet et al., 2008; Wang et al., 2008).  
313 Our own contribution demonstrates that the major uplift occurring during this period was also an  
314 important player in climate changes via hydrologic and ocean dynamics changes. Indeed, we  
315 pinpoint the drastic effect of TP uplift alone on the distribution of the northern hemispheric MOCs  
316 and potentially provide clues for proxy record interpretation.

317 Finally, this simulation is performed with the constant atmospheric CO<sub>2</sub> concentrations at the  
318 pre-industrial, whereas it was higher during the uplift phase in the real world. In the context of past  
319 warm world, such as Late Eocene, the climate conditions are accompanied by high atmospheric  
320 CO<sub>2</sub> concentration, limited sea ice extent, and significantly modified land–sea distribution. Under  
321 these warmer boundary conditions, the responses of AMOC to the TP induced freshwater forcing  
322 may be very different from the modern conditions (e.g., Vavrus and Kutzbach, 2002). Therefore, it  
323 will be necessary to perform further numerical experiments with more realistic boundary conditions  
324 to accurately investigate the contribution of the TP uplift on the oceanic circulation and therefore to  
325 be able to compare with data reconstructions.

326 *Acknowledgements* We sincerely thank the two anonymous reviewers for their insightful  
327 comments and suggestions to improve this manuscript. We also thank Dr. Jiang Zhu for discussions  
328 and technical support during the writing of the paper. This work was supported by the National  
329 Natural Science Foundation of China (41421004, 41572159, and 41625018).

330 Reference

- 331 Abe, M., Kitoh, A., and Yasunari, T.: An evolution of the Asian summer monsoon associated with mountain  
332 uplift—simulation with the MRI atmosphere-ocean coupled GCM, *J. Meteorol. Soc. Jpn.*, 81, 909–933,  
333 2003.
- 334 An, Z., Kutzbach, J. E., Prell, W. L., and Porter, S. C.: Evolution of Asian monsoons and phased uplift of the  
335 Himalaya–Tibetan plateau since Late Miocene times, *Nature*, 411, 62–66, 2001.
- 336 Bolin, B.: On the influence of the earth's orography on the general character of the westerlies, *Tellus*, 2, 184–195,  
337 1950.
- 338 Borrelli, C., Cramer, B. S., and Katz, M. E.: Bipolar Atlantic deepwater circulation in the middle-late Eocene:  
339 Effects of southern ocean gateway openings, *Paleoceanography*, 29, 308–327, 2014.
- 340 Botsyun, S., Sepulchre, P., Risi, C., Donnadieu, Y.: Impacts of Tibetan Plateau uplift on atmospheric dynamics and  
341 associated precipitation  $\delta^{18}\text{O}$ , *Clim. Past*, 12, 1401–1420, 2016.
- 342 Broccoli, A. J., and Manabe, S.: The effects of orography on midlatitude northern hemisphere dry climates, *J.*  
343 *Clim.*, 5, 1181–1201, 1992.
- 344 Chikamoto, M. O., Menviel, L., Abe-Ouchi, A., Ohgaito, R., Timmermann, A., Okazaki, Y., Harada, N., Oka, A.,  
345 and Mouchet, A.: Variability in North Pacific intermediate and deep water ventilation during Heinrich  
346 events in two coupled climate models, *Deep-Sea Res. PT. II*, 61–64, 114–126, 2012.
- 347 Cramer, B. S., Toggweiler, J. R., Wright, J. D., Katz, M. E., and Miller, K. G.: Ocean overturning since the Late  
348 Cretaceous: Inferences from a new benthic foraminiferal isotope compilation, *Paleoceanography*, 24,  
349 PA4216, doi:10.1029/2008PA001683, 2009.
- 350 Cunningham, S. A., Kanzow, T., Rayner, D., Baringer, M. O., Johns, W. E., Marotzke, J., Longworth, H. R., Grant,  
351 E. M., Hirschi, J. J.-M., Beal, L. M., Meinen, C. S., and Bryden, H. L.: Temporal variability of the Atlantic  
352 meridional overturning circulation at 26.5°N, *Science*, 317, 935–938, doi:10.1126/science.1141304, 2007.
- 353 Davies, R., Cartwright, J., Pike, J., and Line, C.: Early Oligocene initiation of North Atlantic deep water formation,  
354 *Nature*, 410, 917–920, 2001.
- 355 DeConto, R. M., and Pollard, D.: Rapid Cenozoic glaciation of Antarctica induced by declining atmospheric CO<sub>2</sub>,  
356 *Nature*, 421, 245–249, 2003.
- 357 DeConto, R. M., Pollard, D., Wilson, P. A., Pälike, H., Lear, C., and Pagani, M.: Thresholds for Cenozoic bipolar  
358 glaciation, *Nature*, 455, 652–657, 2008.
- 359 Dupont-Nivet, G., Hoorn, C., and Konert, M.: Tibetan uplift prior to the Eocene-Oligocene climate transition:  
360 Evidence from pollen analysis of the Xining Basin, *Geology*, 36, 987–990, 2008.
- 361 Emile-Geay, J., Cane, M. A., Naik, N., Seager, R., Clement, A. C., and van Geen, A.: Warren revisited:  
362 Atmospheric freshwater fluxes and “Why is no deep water formed in the North Pacific”, *J. Geophys. Res.*,  
363 108(C6), 3178, doi:10.1029/2001JC001058, 2003.

364 Fallah, B., Cubasch, U., Prömmel, K., and Sodoudi, S.: A numerical model study on the behaviour of Asian  
365 summer monsoon and AMOC due to orographic forcing of Tibetan Plateau, *Clim. Dyn.*, 47, 1485–1495,  
366 2016.

367 Feng, R., and Poulsen, C. J.: Andean elevation control on tropical Pacific climate and ENSO, *Paleoceanography*,  
368 29, 795–809, 2014.

369 Freeman, E., Skinner, L. C., Tisserand, A., Dokken, T., Timmermann, A., Menviel, L., and Friedrich, T.: An  
370 Atlantic–Pacific ventilation seesaw across the last deglaciation, *Earth Planet. Sci. Lett.*, 424, 237–244,  
371 2015.

372 Gent, P. R., Danabasoglu, G., Donner, L. J., Holland, M. M., Hunke, E. C., Jayne, S. R., Lawrence, D. M., Neale,  
373 R. B., Rasch, P. J., Vertenstein, M., Worley, P. H., Yang, Z. L., and Zhang, M.: The Community Climate  
374 System Model version 4, *J. Clim.*, 24, 4973–4991, doi:10.1175/2011JCLI4083.1, 2011.

375 Hague, A. M., Thomas, D. J., Huber, M., Korty, R., Woodard, S. C., and Jones, B. L.: Convection of North Pacific  
376 deep water during the early Cenozoic, *Geology*, 40, 527–530, 2012.

377 Holland, M. M., Bailey, D. A., Briegleb, B. P., Light, B., and Hunke, E.: Improved sea ice shortwave radiation  
378 physics in CCSM4: The impact of melt ponds and black carbon, *J. Clim.*, 25, 1413–1430, 2012.

379 Hu, A., Meehl, G. A., Han, W., Timmermann, A., Otto-Bliesner, B., Liu, Z., Washington, W. M., Large, W.,  
380 Abe-Ouchi, A., Kimoto, M.: Role of the Bering Strait on the hysteresis of the ocean conveyor belt  
381 circulation and glacial climate stability, *Proc. Natl. Acad. Sci. U. S. A.*, 109, 6417–6422, 2012.

382 Jayne, S. R., and Marotzke, J.: A destabilizing thermohaline circulation–atmosphere–sea ice feedback, *J. Clim.*, 12,  
383 642–651, 1999.

384 Jiang, D., Ding, Z. L., Drange, H., and Gao, Y.: Sensitivity of East Asian climate to the progressive uplift and  
385 expansion of the Tibetan Plateau under the mid-Pliocene boundary conditions, *Adv. Atmos. Sci.*, 25,  
386 709–722, 2008.

387 Kitoh, A.: Effects of mountain uplift on East Asian summer climate investigated by a coupled atmosphere–ocean  
388 GCM, *J. Clim.*, 17, 783–802, 2004.

389 Kutzbach, J. E., Prell, W. L., and Ruddiman, W. F.: Sensitivity of Eurasian climate to surface uplift of the Tibetan  
390 Plateau, *J. Geol.*, 101, 177–190, 1993.

391 Liu, X., and Yin, Z.-Y.: Sensitivity of East Asian monsoon climate to the uplift of the Tibetan Plateau, *Palaeogeogr.*  
392 *Palaeoclim. Palaeoecol.*, 183, 223–245, 2002.

393 Maffre, P., Ladant, J. B., Donnadieu, Y., Sepulchre, P., and Godd eris, Y.: The influence of orography on modern  
394 ocean circulation, *Clim. Dyn.*, doi:10.1007/s00382-017-3683-0, 2017.

395 Menviel, L., England, M. H., Meissner, K. J., Mouchet, A., and Yu, J.: Atlantic-Pacific seesaw and its role in  
396 outgassing CO<sub>2</sub> during Heinrich events, *Paleoceanography*, 29, 58–70, 2014.

397 Molnar, P., Boos, W. R., and Battisti, D. S.: Orographic controls on climate and paleoclimate of Asia: Thermal and  
398 mechanical roles for the Tibetan Plateau, *Annu. Rev. Earth. Planet. Sci.*, 38, 77–102, 2010.

399 Nilsson, J., Langen, P., Ferreira, D., and Marshall, J.: Ocean basin geometry and the salinification of the Atlantic  
400 Ocean, *J. Clim.*, 26, 6163–6184, 2013.

401 Okajima, H., and Xie, S. P.: Orographic effects on the northwestern Pacific monsoon: Role of air-sea interaction,  
402 *Geophys. Res. Lett.*, 34, L21708, doi: 10.1029/2007GL032206, 2007.

403 Okazaki, Y., Timmermann, A., Menviel, L., Harada, N., Abe-Ouchi, A., Chikamoto, M. O., Mouchet, A., and  
404 Asahi, H.: Deepwater formation in the North Pacific during the last glacial termination, *Science*, 329,  
405 200–204, 2010.

406 Palmer, T. N., Shutts, G. J., and Swinbank, R.: Alleviation of a systematic westerly bias in general circulation and  
407 numerical weather prediction models through an orographic gravity wave drag parametrization, *Q. J. R.  
408 Meteorol. Soc.*, 112, 1001–1039, 1986.

409 Ramstein, G., Fluteau, F., Besse, J., and Joussaume, S.: Effect of orogeny, plate motion and land-sea distribution  
410 on Eurasian climate change over the past 30 million years, *Nature*, 386, 788–795, 1997.

411 Rind, D., Russell, G., and Ruddiman, W. F.: The effects of uplift on Ocean–Atmosphere, in: *Tectonic Uplift and  
412 Climate Change*, Ruddiman, W. F. (Ed.), Plenum Press, New York, 123–147, 1997.

413 Rodwell, M. J., and Hoskins, B. J.: Subtropical anticyclones and summer monsoons, *J. Clim.*, 14, 3192–3211,  
414 2001.

415 Ruddiman, W. F., and Kutzbach, J. E.: Forcing of Late Cenozoic northern hemisphere climate by plateau uplift in  
416 southern Asia and the American West, *J. Geophys. Res.*, 94(D15), 18409–18427, 1989.

417 Saenko, O. A., Schmittner, A., and Weaver, A. J.: The Atlantic-Pacific seesaw, *J. Clim.*, 17, 2033–2038, 2004.

418 Schmitt, R. W., Bogden, P. S., and Dorman, C. E.: Evaporation minus precipitation and density fluxes for the  
419 North Atlantic, *J. Phys. Oceanogr.*, 19, 1208–1221, 1989.

420 Schmittner, A., Silva, T. A. M., Fraedrich, K., Kirk, E., and Lunkeit, F.: Effects of mountains and ice sheets on  
421 global ocean circulation, *J. Clim.*, 24, 2814–2829, 2011.

422 Seager, R., Battisti, D. S., Yin, J., Gordon, N., Naik, N., Clement, A. C., and Cane, M. A.: Is the Gulf Stream  
423 responsible for Europe's mild winters?, *Q. J. R. Meteorol. Soc.*, 128, 2563–2586, 2002.

424 Sepulchre, P., Sloan, L. C., Snyder, M., and Fiechter, J.: Impacts of Andean uplift on the Humboldt Current system:  
425 A climate model sensitivity study, *Paleoceanography*, 24, PA4215, doi:10.1029/2008PA001668, 2009.

426 Shields, C. A., Bailey, D. A., Danabasoglu, G., Jochum, M., Kiehl, J. T., Levis, S., and Park, S.: The  
427 low-resolution CCSM4, *J. Clim.*, 25, 3993–4014, 2012.

428 Sinha, B., Blaker, A. T., Hirschi, J., Bonham, S., Brand, M., Josey, S., Smith, R. S., and Marotzke, J.: Mountain  
429 ranges favour vigorous Atlantic meridional overturning, *Geophys. Res. Lett.*, 39, L02705,  
430 doi:10.1029/2011GL050485, 2012.

431 Spence, J., Eby, M., and Weaver, A.: The sensitivity of the Atlantic meridional overturning circulation to  
432 freshwater forcing at eddy-permitting resolutions, *J. Clim.*, 21, 2697–2710, 2008.

433 Thomas, D. J.: Evidence for deep-water production in the North Pacific Ocean during the early Cenozoic warm  
434 interval, *Nature*, 430, 65–68, 2004.

435 Thomas, D. J., Korty, R., Huber, M., Schubert, J. A., and Haines, B.: Nd isotopic structure of the Pacific Ocean  
436 70–30 Ma and numerical evidence for vigorous ocean circulation and ocean heat transport in a greenhouse  
437 world, *Paleoceanography*, 29, 454–469, 2014.

438 Vavrus, S., and Kutzbach, J. E.: Sensitivity of the thermohaline circulation to increased CO<sub>2</sub> and lowered  
439 topography, *Geophys. Res. Lett.*, 29, 1546, doi:10.1029/2002GL014814, 2002.

440 Via, R. K., and Thomas, D. J.: Evolution of Atlantic thermohaline circulation: Early Oligocene onset of  
441 deep-water production in the North Atlantic, *Geology*, 34, 441–444, 2006.

442 Wang, C., Zhao, X., Liu, Z., Lippert, P. C., Graham, S. A., Coe, R. S., Yi, H., Zhu, L., Liu, S., and Li, Y.:  
443 Constraints on the early uplift history of the Tibetan Plateau, *Proc. Natl. Acad. Sci. U. S. A.*, 105,  
444 4987–4992, 2008.

445 Warren, B. A.: Why is no deep water formed in the North Pacific?, *J. Mar. Res.*, 41, 327–347, 1983.

446 Weaver, A. J., Bitz, C. M., Fanning, A. F., and Holland, M. M.: Thermohaline circulation: High-latitude  
447 phenomena and the difference between the Pacific and Atlantic, *Annu. Rev. Earth. Planet. Sci.*, 27, 231–285,  
448 1999.

449 Wright, J. D., and Miller, K. G.: Southern ocean influences on late Eocene to Miocene deepwater circulation, in:  
450 The Antarctic Paleoenvironment: A perspective on global change part two, Kennett, J. P. and Warnke, D. A.  
451 (Eds.), American Geophysical Union, Washington, 1–25, 1993.

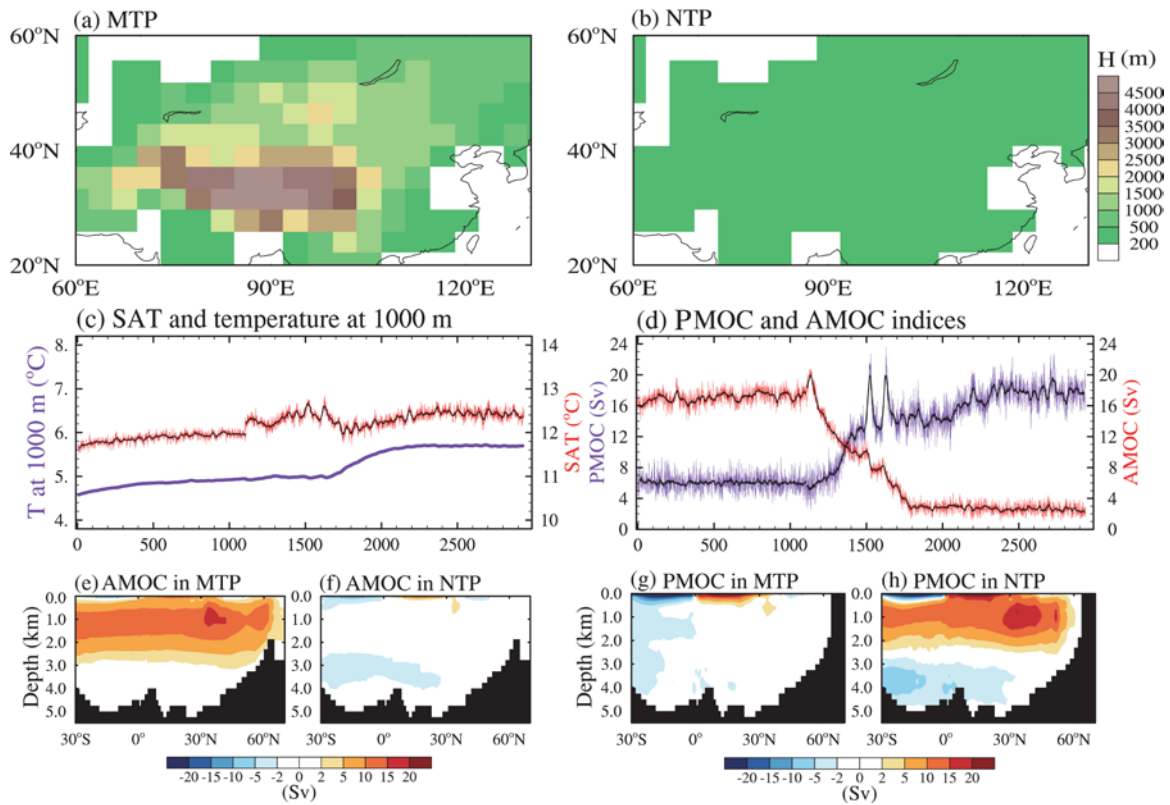
452 Zachos, J., Pagani, M., Sloan, L., Thomas, E., and Billups, K.: Trends, rhythms, and aberrations in global climate  
453 65 Ma to present, *Science*, 292, 686–693, 2001.

454 Zachos, J. C., Dickens, G. R., and Zeebe, R. E.: An early Cenozoic perspective on greenhouse warming and  
455 carbon-cycle dynamics, *Nature*, 451, 279–283, 2008.

456 Zhang, R., Jiang, D., Zhang, Z., and Yu, E.: The impact of regional uplift of the Tibetan Plateau on the Asian  
457 monsoon climate, *Palaeogeogr. Palaeoclim. Palaeoecol.*, 417, 137–150, 2015.

458 Zhang, Z., Nisancioglu, K. H., Flatoy, F., Bentesen, M., Bethke, I., and Wang, H.: Tropical seaways played a more  
459 important role than high latitude seaways in Cenozoic cooling, *Clim. Past*, 7, 801–813, 2011.

460 Zhu, J., Liu, Z., Zhang, X., Eisenman, I., and Liu, W.: Linear weakening of the AMOC in response to receding  
461 glacial ice sheets in CCSM3, *Geophys. Res. Lett.*, 41, 6252–6258, 2014.



462

463

464

465

466

467

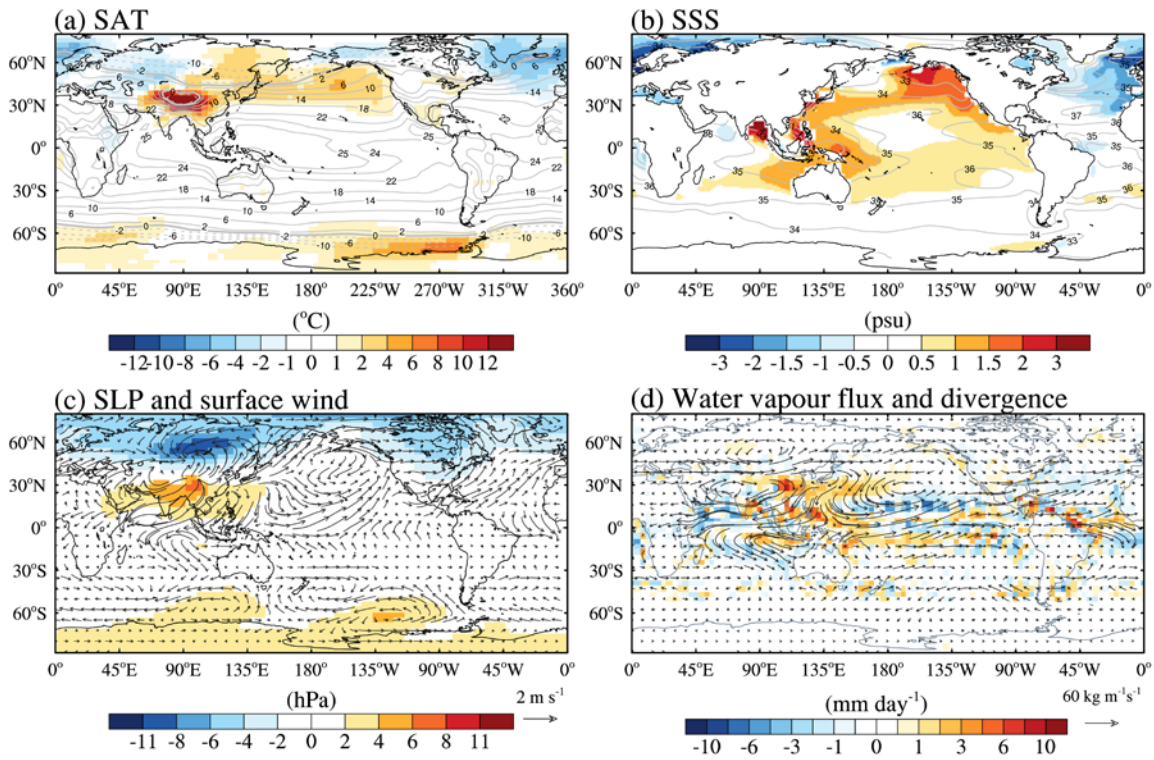
468

469

470

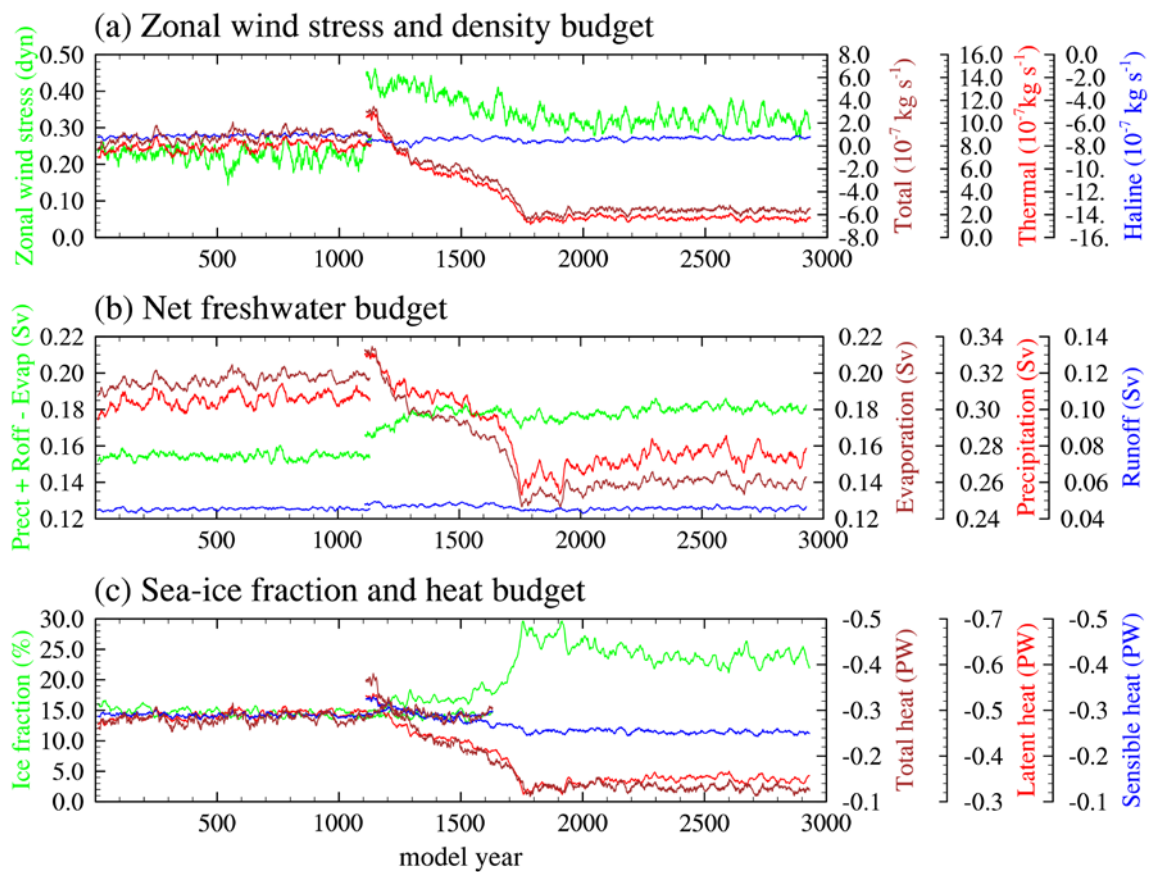
471

**Figure 1.** Two topographic height configurations used in experiments: (a) MTP and (b) NTP. (c) Time series of global mean annual 2-m surface air temperature (SAT) and sea temperature at 1000 m depth in MTP (1–1100 years) and NTP (1101–2940 years) simulations; bold black lines show 21-year running mean. (d) Same as (c) but for PMOC and AMOC indices, respectively. AMOC and PMOC indices are defined as the annual maximum of the meridional stream function value north of 28°N and below the depth of 500 m over the North Atlantic and Pacific, respectively. (e–h) Climatological annual mean Atlantic and Indian–Pacific meridional overturning stream function in MTP (e and g) and NTP (f and h); positive (negative) shading represents clockwise (counterclockwise) circulations.



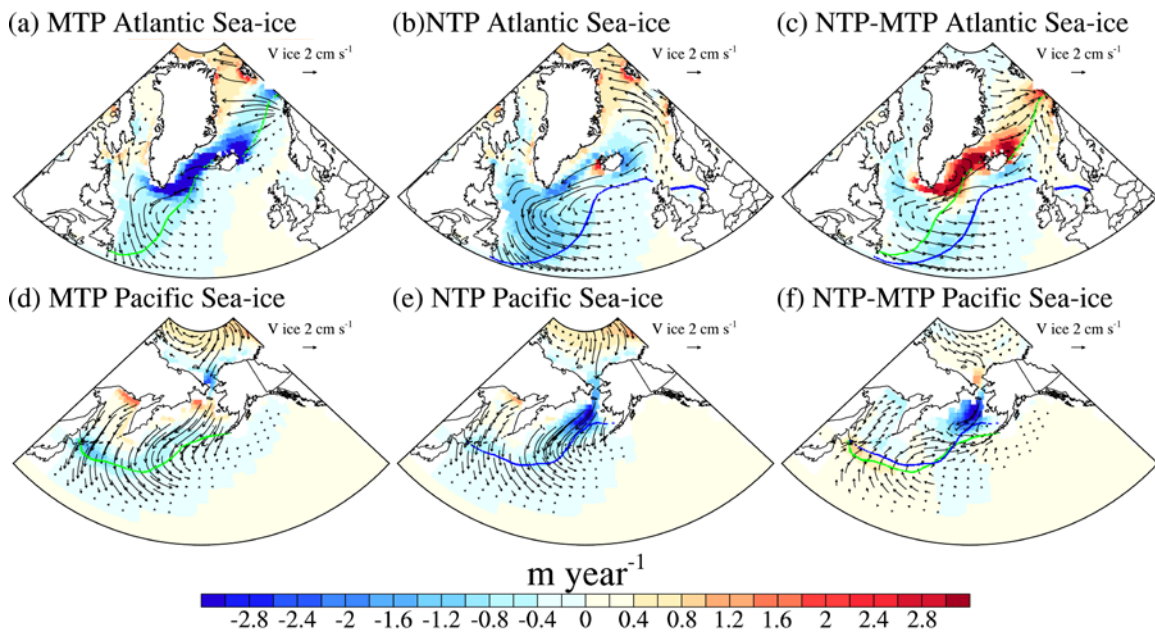
472

473 **Figure 2.** (a) Climatological SAT in MTP (contour) and anomalies (shaded) for NTP minus MTP;  
 474 (b) same as Figure 2a, but for sea surface salinity (SSS); (c) changes in sea-level pressure (SLP,  
 475 shading) and surface wind (vectors); and (d) vertically integrated (surface to 300 hPa pressure layer)  
 476 water vapor flux (vectors) and its convergence (shading) in NTP relative to MTP. Unit of  
 477 convergence is converted to  $\text{mm day}^{-1}$  assuming the density of liquid water as  $1 \text{ g cm}^{-3}$ .



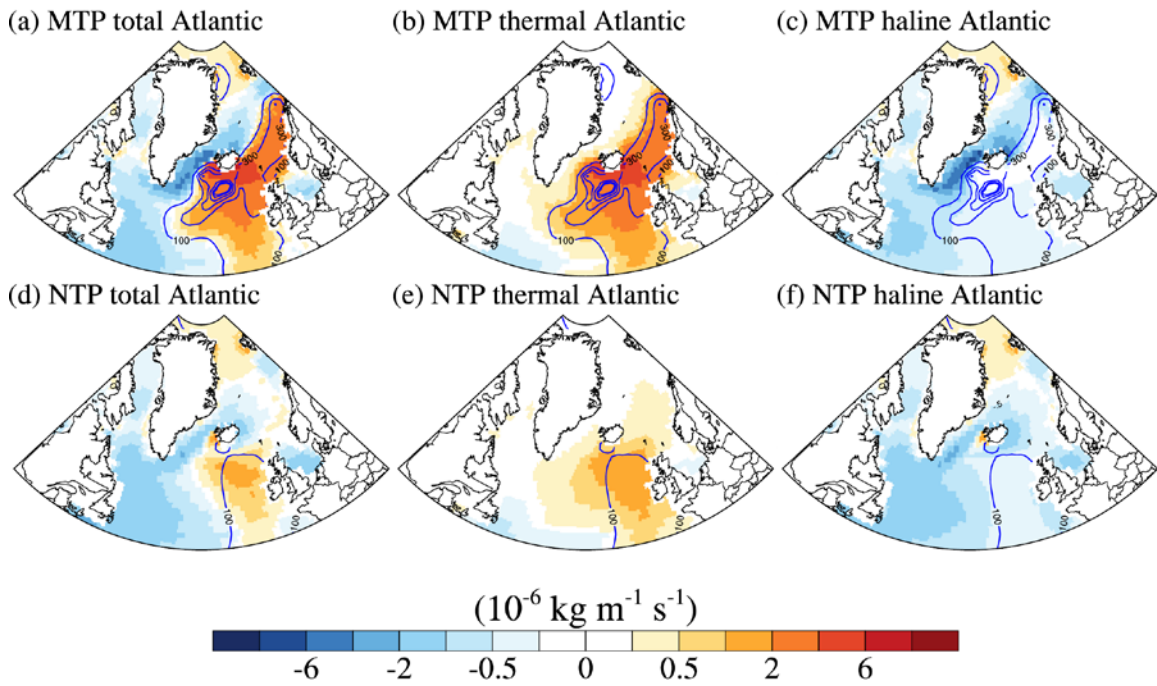
478

479 **Figure 3.** Regional annual mean across North Atlantic basin at 40°–70°N for MTP (1–1100 years)  
 480 and NTP (1101–2940 years) of (a) zonal surface wind-stress, total density flux, haline density flux,  
 481 and thermal density flux (total density flux is decomposed into haline contribution due to freshwater  
 482 flux and thermal contribution due to heat flux (*Schmitt et al.*, 1989); (b) net freshwater, precipitation,  
 483 runoff, and evaporation fluxes; (c) sea-ice fraction, total heat, sensible heat, and latent heat fluxes,  
 484 (units: PW, 1 PW =  $10^{15}$  W). For comparison purposes, all lines with common units use identical  
 485 vertical scale spacing.



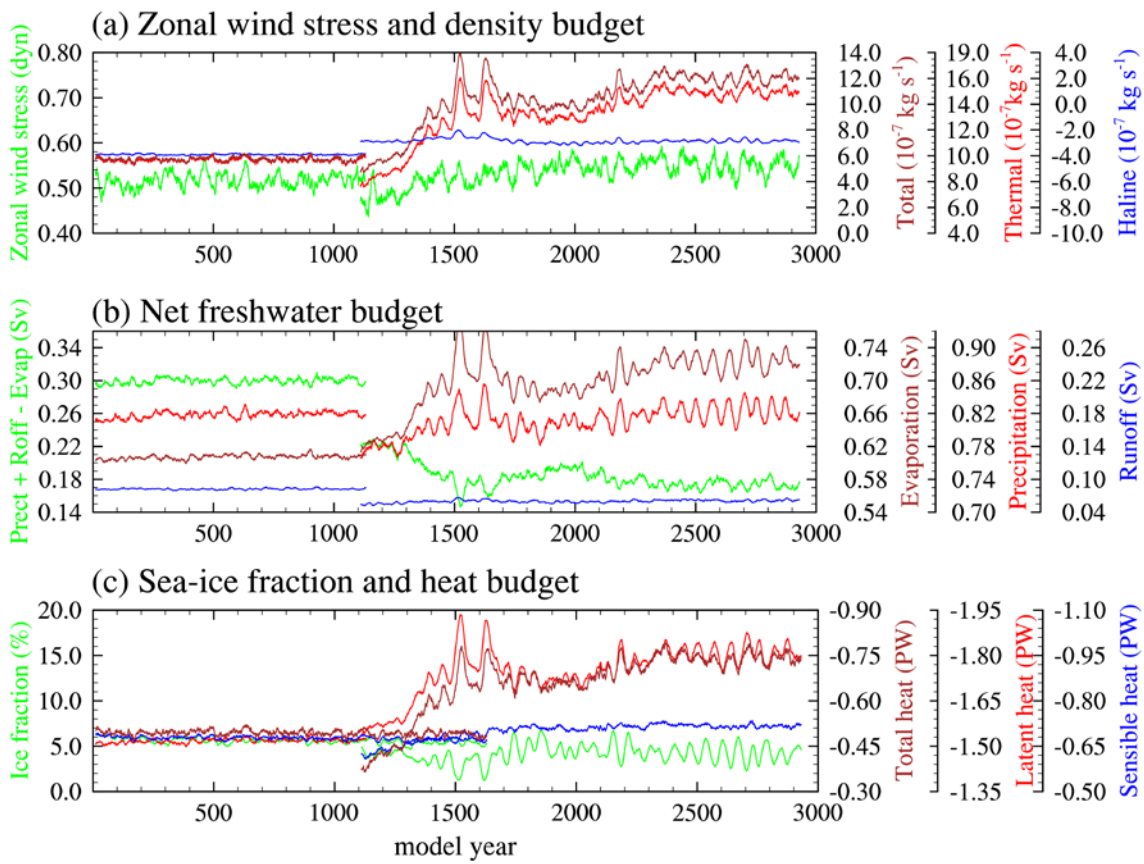
486

487 **Figure 4.** The North Atlantic and Pacific region features of annual mean sea-ice formation rate  
 488 (shading; positive stands for formation, and negative stands for melting), sea-ice velocity (vectors,  
 489  $\text{cm s}^{-1}$ ), and for (a, d) MTP, (b, e) NTP, and (c, f) difference between NTP and MTP. The February  
 490 sea-ice margin is indicated with dashed lines (defined as the 15% sea-ice coverage, green line for  
 491 MTP, blue line for NTP)



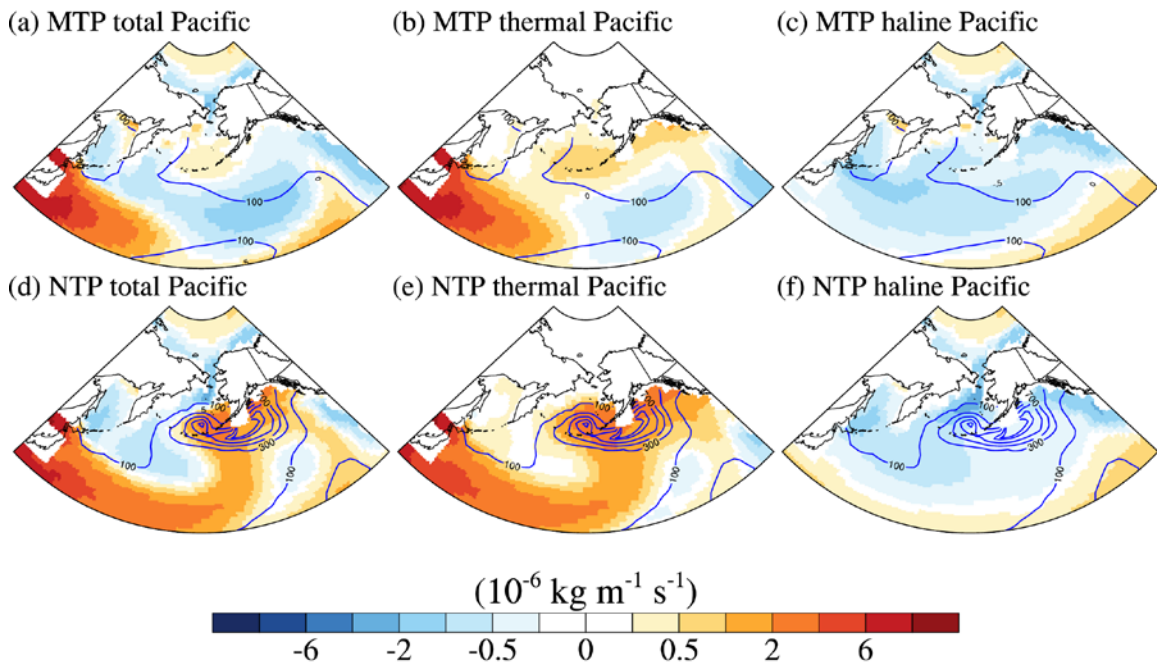
492

493 **Figure 5.** The North Atlantic annual mean (a, d) total density flux (shading; positive means flux  
 494 makes water denser), (b, e) the thermal density flux, (c, f) the haline density flux, and the winter  
 495 mixed layer depth (blue contour, contour interval: 200 m) in the MTP (upper panel) and NTP (lower  
 496 panel).



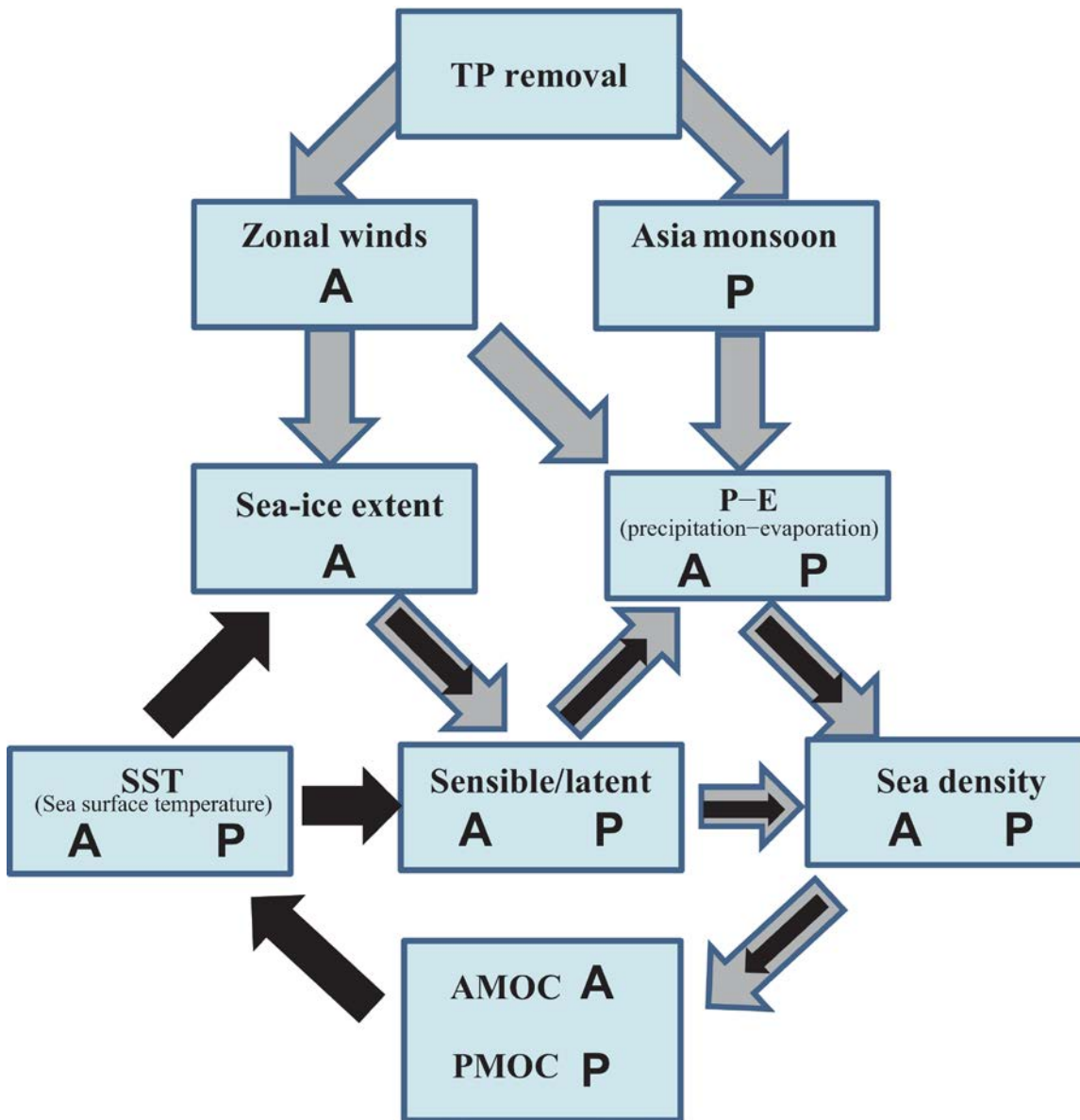
497

498 **Figure 6.** As in Figure 3, but for North Pacific basin at 30°–70°N.



499

500 **Figure 7.** The same as Figure 5, but for the North Pacific (30–80°N).



501

502 **Figure 8.** Schematic diagram about the influence of the removal of TP on the AMOC and PMOC.

503 Vectors in gray denote the climate responses in relation to the increased in wind-induced and  
 504 decreased monsoonal-driven net precipitation-evaporation and wind-driven sea-ice processes. The

505 black color vectors denote the feedback processes. The bold characters A and P stand for the

506 physical processes occurring over the North Atlantic and Pacific, respectively.

The last marked-up manuscript version-20180321 relative to the original version-20170831:

# 1 **Intensified Atlantic vs. weakened Pacific meridional overturning** 2 **circulations in response to Tibetan Plateau uplift**

3 Baohuang Su<sup>1,4</sup>, Dabang Jiang<sup>1,2,3,4</sup>, Ran Zhang<sup>1</sup>, Pierre Sepulchre<sup>5</sup>, and Gilles Ramstein<sup>5</sup>

4 <sup>1</sup>Institute of Atmospheric Physics, Chinese Academy of Sciences, Beijing 100029, China

5 <sup>2</sup>Joint Laboratory for Climate and Environmental Change at Chengdu University of Information Technology,  
6 Chengdu 610225, China

7 <sup>3</sup>CAS Center for Excellence in Tibetan Plateau Earth Sciences, Beijing 100101, China

8 <sup>4</sup>University of Chinese Academy of Sciences, Beijing 100049, China

9 <sup>5</sup>Laboratoire des Sciences du Climat et de l'Environnement/IPSL, CEA-CNRS-UVSQ, UMR8212, Orme des  
10 Merisiers, CE Saclay, 91191 Gif-sur-Yvette Cedex, France

11 **Abstract:** The role of the Tibetan Plateau (TP) in maintaining the large-scale overturning  
12 circulation in the Atlantic and Pacific is investigated using a coupled atmosphere–ocean model.  
13 For the present day with a realistic topography, model simulation shows a strong Atlantic  
14 meridional overturning circulation (AMOC) but a near absence of a-the Pacific meridional  
15 overturning circulation (PMOC), which is-are in good agreement with the present observations. In  
16 contrast, the simulation without the TP depicts a collapsed AMOC and a strong PMOC that  
17 dominates deep water formation. The switch in deep water formation between the two basins  
18 results from changes in the large-scale atmospheric circulation and atmosphere–ocean feedback in  
19 over the Atlantic and Pacific. The intensified westerly winds and increased freshwater flux over

20 the North Atlantic cause an initial slowdown of the AMOC, ~~but~~ while the weakened East Asian  
21 monsoon circulation and associated decreased freshwater flux over the North Pacific ~~enhance~~ give  
22 rise to the initial intensification of the PMOC. The further decreased heat flux and the associated  
23 increase in sea-ice fraction promote the final AMOC collapse over the Atlantic, while the further  
24 increased heat flux leads to the final PMOC establishment over the Pacific. Although the  
25 simulations were done in a cold world, it still importantly implicates that the uplift of the TP alone  
26 could have been a potential driver for the reorganization of PMOC–AMOC between the Late  
27 Eocene and Early Oligocene.

## 28 1. Introduction

29 The uplift of the Tibetan Plateau (TP) ~~was~~ a major tectonic event that ~~has~~ had occurred  
30 throughout the Cenozoic, and its gradual growth ~~had~~ exerted a strong influence on the  
31 atmospheric circulation and climate (Molnar et al., 2010). Since the pioneering work of Bolin  
32 (1950), the impacts of mountain uplift on regional and global climate have been extensively  
33 investigated ~~by a large body of studies~~. Nevertheless, ~~although~~ most studies have emphasized the  
34 role of mountain ranges on atmosphere dynamics, while quantifications of the associated impact  
35 on ocean dynamics have been rare. For example, most previous works have taken atmospheric  
36 general circulation models to address regional climate effects, notably the Asian monsoon and  
37 arid environment evolutions (e.g., Ruddiman and Kutzbach, 1989; Ramstein et al., 1997; An et al.,  
38 2001; Liu and Yin, 2002; Jiang et al., 2008; Zhang et al., 2015). However, simulations have  
39 recently been applied to investigate the effect of mountain uplift in the context of the  
40 atmosphere–ocean system, and a few studies have proposed that the uplift of the Andes  
41 (Sepulchre et al., 2009) and Rocky Mountains (Seager et al., 2002) is closely linked to the

42 evolution of oceanic circulations, including the Gulf Stream and Humboldt Current, and the El  
43 Niño–Southern Oscillation system (Feng and Poulsen, 2014). Although it has been indicated that  
44 the TP uplift affects sea surface temperatures, sea surface salinity, precipitation, and trade winds  
45 for both the Pacific and equatorial Indian Ocean (Abe et al., 2003; Kitoh, 2004; Okajima and Xie,  
46 2007), the influence of the TP uplift on the high-latitude ~~ocean circulation~~oceanic circulations,  
47 particularly in the North Atlantic, has rarely been explored.

48 The potential importance of mountain uplift in modifying the oceanic thermohaline  
49 circulation has previously been investigated. Ruddiman and Kutzbach (1989) indicated that  
50 mountain uplift-induced changes in the North Atlantic surface circulation are expected to increase  
51 the North Atlantic Deep Water formation. In addition, Rind et al. (1997) performed the coupled  
52 model simulations with and without TP and proposed that the TP may have a considerable impact  
53 on the large-scale meridional overturning circulation (MOC). However, the integration time used  
54 in this pioneering simulations was too short to fully evaluate the deep oceanic circulation response,  
55 and thus ~~more studies are still needed to quantify~~evaluate~~no previous study has yet quantified~~ the  
56 possible role of the TP in modulating ~~on~~ the MOC.

57 On a geological timescale, remarkable reorganization and evolution of the large-scale  
58 oceanic overturning circulation, from the Southern Ocean deep water dominating mode to the  
59 modern-like North Atlantic deep water mode, have been evidenced through the Late Eocene to the  
60 Early Oligocene (Wright and Miller, 1993; Davies et al., 2001; Via and Thomas, 2006). This  
61 dramatic shift is possibly associated with major rearrangements in the ocean seaways and other  
62 tectonic changes, although the ultimate trigger is still being debated (Zhang et al., 2011). In  
63 addition, ~~)- various lines of investigation~~it is have suggested that the regional surface of the TP  
64 haved reached a high elevation of more than 4000 meters around 40 Ma ago (Dupont-Nivet et al.,

65 [2008; Wang et al., 2008](#)), although debates regarding paleoaltitude reconstructions remain  
66 [\(Botsyun et al., 2016\)](#). Given ~~the~~ this timing of TP uplift ~~(Wang et al., 2008; Molnar et al., 2010)~~,  
67 it is important to quantify the contribution of TP uplift on the meridional oceanic circulation of  
68 the Northern Hemisphere. In this study, therefore, two coupled atmosphere–ocean numerical  
69 integrations, with and without TP, are designed to investigate the role of the TP on the Atlantic  
70 MOC (AMOC) and Pacific MOC (PMOC). ~~Due to the length of these coupled simulations, here~~  
71 ~~we restrict our analysis to the sensitivity of the TP uplift without modifying other parameters.~~

## 72 2. Model, experimental design, and density flux analysis

### 73 2.1. Model and experiments

74 The Community Earth System Model (CESM) version 1.0.5 of the National Center for  
75 Atmospheric Research is a widely used, well-validated coupled model with dynamic atmosphere,  
76 land, ocean, and sea-ice components (Gent et al., 2011). It is applied to this study at a  
77 low-resolution configuration that is computationally efficient and well-described (Shields et al.,  
78 2012) and employs an atmospheric horizontal grid of roughly  $3.75^\circ \times 3.75^\circ$  (T31) with 26 vertical  
79 levels. The ocean model adopts a finer oceanic horizontal grid, with a nominal  $3^\circ$  resolution  
80 increasing to  $1^\circ$  near the equator ( $116 \times 100$  grid points, latitude by longitude) and 60 unevenly  
81 spaced layers in the vertical direction. The sea-ice and land models share the same horizontal  
82 grids as the ocean and atmosphere models, respectively, where the sea-ice component is a  
83 dynamic–thermodynamic model that includes a subgrid-scale ice thickness distribution and  
84 energy-conserving thermodynamics (Holland et al., 2012).

85 Two experiments are conducted; firstly, a control run with the modern topography (MTP,  
86 Figure 1a), and secondly a sensitivity run where topography within the region of  $20^\circ\text{--}60^\circ\text{N}$  and

87 60<sup>o</sup>→140°E at altitudes higher than 200 m is set to 200 m (NTP, Figure 1b), which enables  
88 examination of the climate effect in relation to the TP topography. This TP uplift configuration  
89 has been referred to in the majority of previous simulation works (e.g., Liu and Yin, 2002; Jiang et  
90 al., 2008). This greatly simplified topographic setting is not intended to represent a realistic  
91 scenario constrained by the geological evidence and instead represents two end-members of the  
92 potential growth histories of the TP. So, it is important to note that these experiments only aim to  
93 investigate the TP uplift occurring in “a cold world” with an atmospheric CO<sub>2</sub> corresponding to  
94 the pre-industrial values (284.0 ppm). With the exception of topography, all the other boundaries,  
95 such as ~~land-sea~~continent-ocean distributions and orbital parameters, are prescribed to  
96 pre-industrial conditions. The MTP is continually integrated for 1100 years, and the NTP is  
97 additionally integrated for another 1840 years starting from the year 1100 of the MTP. Global  
98 mean surface air temperature and sea temperature at a depth of 1000 m are shown in Figure 1c.  
99 Both simulations reach ~~an~~ equilibrium states after more than 1000 model years of integration time,  
100 and the final 200 years of both cases are applied for our climate state analysis.

## 101 2.2. Density flux analysis

102 Because one of the major aims of this paper is to analyze ~~the~~ changes in the meridional  
103 oceanic circulation, we decided to focus on the density flux parameter, which is appropriate to  
104 diagnose these oceanic circulation changes. The dense deep water masses are formed in the area  
105 with relatively high surface density achieved by cooling or increasing salinity. To better  
106 understand which processes dominated the MOC changes in simulations, it is instructive to  
107 further analyze the time evolution of density fluxes budget. Therefore, a density flux analysis  
108 method, in which the total density flux decomposes into the haline contribution due to freshwater

109 flux and the thermal contribution due to heat flux (Schmitt et al., 1989), is adopted in our study.

110 The total density flux is calculated from a linearized state equation of seawater, as

$$F_{\rho} = -\alpha \cdot \frac{Q}{C_p} + \rho(\mathbf{0}, T) \cdot \beta \cdot \frac{(E - P - R - I) \cdot S}{1 - S}$$

111  $F_{\rho}$  is the total density flux,  $-\alpha \cdot \frac{Q}{C_p}$  is thermal density flux, and  $\rho(\mathbf{0}, T) \cdot \beta \cdot \frac{(E - P - R - I) \cdot S}{1 - S}$  is

112 haline density term.  $C_p$ ,  $T_s$  and  $S$  are the specific heat capacity, surface temperature and salinity

113 of seawater, respectively.  $\alpha$  and  $\beta$  are the thermal expansion and haline contraction coefficients,

114 respectively.  $\rho(\mathbf{0}, T)$  is the density of freshwater with a salinity of 0 psu and temperature of  $T$ .

115  $Q$  represents the net surface heat flux.  $E$ ,  $P$ ,  $R$ , and  $I$  denote the freshwater fluxes due to

116 evaporation, precipitation, river runoff, and sea-ice melting (or brine rejection), respectively.

### 117 3. Results

#### 118 3.1. Changes in AMOC and PMOC

119 There are evident changes in the AMOC and PMOC indices in response to the TP uplift

120 (Figure 1d). With MTP, the AMOC stabilizes at around 17 Sv ( $\text{Sv} = 10^6 \text{ m}^3 \text{ s}^{-1}$ ) for more than

121 1000 years (Figure 1d, 1–1100 years, red line), which agrees with the observations 18.7 ± 5.6 Sv

122 for 2004–2005 (Cunningham et al., 2007), but with NTP there is a continual weakening of the

123 AMOC until the point of quasi-collapse (ca. 2 Sv, Figure 1d). In contrast, the PMOC of NTP

124 begins at a sluggish level from MTP (Figure 1d, 1–1100 years, purple line) and takes as long as

125 1200 years to reach an equilibrium state that is comparable to the level of the AMOC in MTP (ca.

126 18 Sv, Figure 1d, 1101–2940 years, purple line). In agreement with the dramatic responses of

127 AMOC and PMOC, sea surface salinity increases in the North Pacific but decreases in a broad

128 area of the North Atlantic (Figure 2b). To fully understand the different behaviors between AMOC

129 and PMOC in NTP, in the following sections we further analyze ~~the~~ changes in the atmospheric

130 and oceanic circulations and the atmosphere–ocean feedbacks.

### 131 3.2. Atmospheric responses

132 The modified AMOC and PMOC are linked to the large-scale atmospheric circulation  
133 changes. In terms of model results of the NTP relative to the MTP, the surface air temperature  
134 over and around the TP and in the North Pacific increased but decreased over the North Atlantic  
135 (Figure 2a), which agrees with the previous simulations (Broccoli and Manabe, 1992; Kutzbach et  
136 al., 1993). In addition, there are intensified westerlies over the North Atlantic and weakened  
137 subtropical anticyclones and trade winds over the North Pacific (Figure 2c); the former results  
138 from a significant increase in the meridional pressure gradient driven by a large-scale  
139 equatorward shift of air mass occupying the current position of the TP (Figure 2c) and from a  
140 reduced drag of the orographically induced gravity waves associated with the absence of the TP  
141 (Palmer et al., 1986; Sinha et al., 2012), ~~whereas~~ while the latter is derived from the weakening of  
142 zonal Eurasia–Pacific thermal contrast in the middle troposphere (not shown), especially in boreal  
143 summertime, in relation to removal of the mountains (Ruddiman and Kutzbach, 1989; Rodwell  
144 and Hoskins, 2001; Kitoh, 2004).

145 When the TP is removed, the atmospheric moisture transport between the Pacific and  
146 Atlantic Oceans undergoes a basin-basin asymmetric redistribution as a response to the  
147 large-scale circulation anomalies (Figure 2c). In comparison with MTP results, the NTP  
148 simulation shows large amounts of anomalous westerly moisture flux transported through the  
149 lowlands of Central America to the North Atlantic, causing weak moisture convergence therein  
150 (Figure 2d). In addition, removal of the TP leads to a significant divergence of moisture over East  
151 Asia and the western North Pacific marginal seas (Figure 2d), which is linked to a weakened

152 monsoon circulation and is consistent with the previous simulations using both atmospheric and  
153 coupled ocean–atmosphere general circulation models (Liu and Yin, 2002; Kitoh, 2004; Molnar et  
154 al., 2010). The anomalies of atmospheric circulation shown above are derived partially from the  
155 positive feedback caused by the changed sea surface temperature due to the removal of the TP. In  
156 More importantly particular, this the weakening of both the Asian monsoon-collapse and associated  
157 with TP removal was North Pacific subtropical anticyclone in association with the TP removal  
158 were previously shown to more aggravated be greater in the context of coupled models as  
159 compared to that in atmosphere–atmosphere-alone-only models due to the enhanced additional  
160 ocean–atmosphere feedback (Kitoh, 2004). Thus, the atmosphere–ocean feedbacks also play an  
161 important role in maintaining the inter-basin atmospheric moisture asymmetric  
162 redistribution. Meanwhile, the freshwater discharge around the western North Pacific marginal  
163 seas from the Asian rivers was previously found to be substantially reduced in response to  
164 monsoon-collapse (Kitoh et al., 2010).

### 165 3.3. Oceanic responses and atmosphere–ocean feedbacks

#### 166 3.3.1. Changes in freshwater and sea-ice

167 The above changes in the large-scale atmospheric circulation markedly decrease the total  
168 ocean density flux in the North Atlantic (Figure 3a, brown), supporting the trend of the AMOC  
169 (Figure 1d). Both the increases of net freshwater and wind-driven sea-ice expansion are  
170 responsible for the initial reduction of total ocean density flux and further induce a gradual  
171 weakening of the AMOC. In more details, on the one hand, the anomalous atmospheric  
172 circulation associated with the removal of the TP drives more water vapor transportation  
173 northward (Figure 2d) over the North Atlantic Ocean, causing more precipitation at the beginning

174 of NTP simulation (Figure 3b, ca. 1101–1200 years, red line). Correspondingly, the net freshwater  
175 flux (precipitation plus runoff minus evaporation) convergence into the North Atlantic basin at  
176 40°–70°N increases by 0.005 Sv (~3%) and 0.025 Sv (~16%) at the initial and final states of NTP  
177 simulations (Figure 3b, green), respectively. ~~On the other hand~~ Moreover, there is a significant  
178 increase in the area-averaged sea-ice coverage over the North Atlantic through wind-driven  
179 processes (Figure 3c, green). With the TP, the annual mean sea-ice forms mainly in the northern  
180 and western region of the sub-polar North Atlantic, and it shifts southward and eastward when  
181 driven by cyclonic wind stress associated with the Icelandic Low, and melts in the Labrador Sea  
182 (sub-polar gyre) caused by a warm condition (Figure 4a). By comparison, after removal of the TP,  
183 anomalously intensified cyclonic winds induce an anomalous eastward sea-ice velocity (Figure  
184 4c), and cause a rapid eastward shift of the sea-ice margin (Figure 4c). Meanwhile, the locally  
185 melted sea-ice due to thermodynamics processes reduces in the southeast of Greenland (red  
186 shading, Fig. 4c), but increases in the south of Greenland (blue shading, Fig. 4c). It suggests that  
187 there is ~~much~~ more sea-ice transporting from the high latitudes into the sub-polar gyre region, and  
188 the anomalous expansion of sea-ice margin in this region primarily originates from the  
189 wind-driven eastward transportation (dynamics processes), but not the local formation  
190 (thermodynamic processes). Because of this increased sea-ice through thermodynamically  
191 insulating the sea water from the freezing air, the release of sensible and latent heat into the  
192 atmosphere decreases and the density of sea water finally reduces, which processes have also  
193 been previously elucidated by Zhu et al. (2014).

194 Moreover, the total ocean density flux increases in the North Pacific in response to the  
195 removal of the TP. Due to the weakened Asian monsoon circulation and associated decrease in  
196 rainfall and runoff after lowering the topography, the net freshwater flux received by the North

197 Pacific decreases by 0.08 Sv (~26%) and 0.12 Sv (~40%) during the initial and end stages of the  
198 NTP simulation, respectively (Figure 6b, green). This continuous negative freshwater flux forcing  
199 tends to increase density and initially leads to the formation of the North Pacific dense water,  
200 which is verified from changes in the haline density flux (Figure 6a). Specifically, during the first  
201 200 years of the NTP run, the haline density flux constantly produces a net positive contribution  
202 to the total density relative to the MTP haline term (Figure 6a, blue line). Meanwhile, the thermal  
203 density flux remains at a lower level (Figure 6a, ca. 1101–1300 years, red line) relative to the  
204 MTP. Thus, it indicates that the initially increased density of the North Pacific is largely attributed  
205 to the haline density term, but not the thermal density term.

### 206 3.3.2. Roles of the atmosphere–ocean feedbacks

207 The aforementioned weakening of the AMOC due to the atmospheric processes further  
208 triggers a positive atmosphere–ocean feedback loop through reducing northward heat transport,  
209 and subsequent decreasing sea surface temperatures, then allowing sea-ice to expand, suppressing  
210 the releasing of evaporating latent and sensible heat, and reducing the sea water density, and  
211 further weakening the AMOC, as previously shown in Jayne and Marotzke (1999) and Zhu et al.  
212 (2014). Note that the negative effect of net freshwater becomes increasingly unimportant  
213 compared to the heat flux feedback associated with the latent/sensible heat changes (Figure 3a).  
214 Finally, the thermal density flux decreases by 49% relative to the MTP run, which substantially  
215 dominates the total density flux changes (Figure 3a). To be specific, the annual mean total density  
216 flux and mixed layer depth over the North Atlantic, especially around the Iceland where the  
217 collapse of deep water formation occurs, is dramatically decreased in NTP (Figure 5d, the  
218 maximum mixed layer depth is approximately about 100 m) in comparison to that in MTP (Figure

219 5a, the maximum mixed layer depth is approximately 900 m). Moreover, this reduced total  
220 density flux over the North Atlantic is more attributed to the decreased thermal density flux  
221 associated with less latent and sensible released (Figure 5e) than the changed haline density flux  
222 (Figure 5f).

223 Atmosphere–ocean feedbacks also strengthen the PMOC. Due to the initial development of  
224 the PMOC mentioned in section 3.1, a positive feedback (as pointed out in Warren (1983)) is  
225 initiated by the intensifying meridional oceanic circulation; this transports warmer subtropical  
226 water northward and leads to the buoyancy loss and evaporation increase (Figure 6b). This  
227 feedback is also able to re-trigger PMOC enhancement. By comparison to the changes in the  
228 North Atlantic, both the regionally averaged sea-ice coverage (Figure 6c) and February sea-ice  
229 margin (Figure 4f) over the North Pacific experience a slightly northward retreat and have a  
230 relatively smaller effect on the simulated strengthening of the PMOC. Over a longer time, the  
231 thermal density flux, which is due to the loss of total heat, contributes more to the total density  
232 flux than the haline flux in relation to reduction in the net freshwater discharge (Figure 6b).  
233 Spatially, both increased total density flux and mixed layer depth in the North Pacific Ocean show  
234 opposite change characteristics with the North Atlantic (Figure 7d). Correspondingly, in  
235 comparison to the MTP, there is a widespread increase of the thermally induced density flux in the  
236 sub-polar North Pacific in NTP (Figure 7f), but with little spatially changed in the haline density  
237 flux (Figure 7f). Thus, in contrast to the results shown in the North Atlantic, the increased total  
238 heat exchange between the atmosphere and ocean due to the processes of sensible and latent heat  
239 releases (Figure 6b) ultimately becomes a dominant factor in maintaining a vigorous PMOC by  
240 controlling the increased total density flux (Figure 6a).

#### 241 4. Conclusions and Discussion

242 This study investigates the effect of TP uplift on [the](#) large-scale oceanic circulation using a  
243 low-resolution version of CESM. Results show that the removal of the TP initially changes the  
244 wind-driven atmospheric moisture transport process and the wind-driven sea-ice coverage  
245 expansion process, which are responsible for the initial weakening of [the](#) AMOC. Meanwhile, the  
246 suppressed monsoonal circulation in East Asia and [the](#) western Pacific marginal seas induces the  
247 decrease of rainfall and runoff and further causes the initially increased PMOC. Moreover, the  
248 positive feedback further changes [the](#) AMOC and PMOC. In particular, the AMOC weakening  
249 can further decrease [the](#) North Atlantic sea surface temperatures, ocean–atmosphere temperature  
250 contrast, evaporation, and precipitation, and subsequently increase sea-ice coverage. These  
251 processes together cause the final changes of [the](#) AMOC and PMOC (Figure 8).

252 A previous study demonstrated the role of Rocky Mountain uplift on heat transport and Gulf  
253 Stream patterns in the North Atlantic (Seager et al., 2002). In this study, we focus on the most  
254 prominent long-term orogenesis occurring since the Eocene: the TP and Himalayan uplift and  
255 associated impacts on the MOC. Our results can be compared with those derived from [the](#) earlier  
256 simulations, although experimental configurations differ somewhat. It has been indicated that [the](#)  
257 removal of global mountains triggers the collapse of deep water in the North Atlantic but enables  
258 formation in the North Pacific in [two](#) different coupled models (Schmittner et al., 2011; Sinha  
259 et al., 2012; Maffre et al., 2017). The simulated weakening of the AMOC is also qualitatively  
260 consistent with recent experiments using a decreased elevation of the TP and Central Asia (Fallah  
261 et al., 2016). However, only TP topography is reduced in our study, but our results are comparable  
262 with those of [the](#) past studies, therefore highlighting the key role that TP has played in forming  
263 the current large-scale deep oceanic circulation pattern. Nevertheless, given that all existing

264 simulations (including ours) have used a rather coarse resolution of the coupled model  
265 configuration, it is considered that a finer resolution model may provide a better representation of  
266 the western boundary currents and allow for a more accurate and realistic resolving of the ocean  
267 eddies, which are believed to be critically important oceanic processes that should be taken in the  
268 realistic simulations of the AMOC (Spence et al., 2008). In addition, the low-resolution CESM is  
269 also generally found to generally have a cold bias with the underestimated ocean heat transport  
270 and excessive Arctic sea-ice (Shields et al., 2012), which could potentially exert modulations on  
271 the AMOC weakening. It is thus considered that investigating the response of the PMOC and  
272 AMOC to the TP uplift using an atmosphere–ocean general circulation model with a higher  
273 spatial resolution would be useful. Besides, the robust changes in the AMOC and PMOC, and the  
274 associated mechanisms due to the TP uplift can be ~~evaluated~~~~achieved~~ through multi-model  
275 comparison.

276 Based on a comprehensive analysis of modern climatological data, Warren (1983) and  
277 Emile-Geay et al. (2003) hypothesized that the present MOC (mainly occurring in the Atlantic but  
278 not in the Pacific) is determined by the large mountains, namely the Himalayas and Rockies,  
279 which induce an asymmetric distribution of wind stress and moisture transport features between  
280 the Atlantic and Pacific basins. However, previous studies have also demonstrated that the  
281 asymmetric continental extents and basin widths (basin geometries) between the two basins  
282 (Weaver et al., 1999; Nilsson et al., 2013) also play a possible key role in maintaining the present  
283 day AMOC. Our simulations support ~~this-the~~ hypothesis based on proposed by Warren (1983) and  
284 highlight the significant role of the TP alone in ~~supporting~~maintaining the modern AMOC.  
285 Moreover, the Similar-similar PMOC–AMOC seesaw dynamics have also been ~~determined~~~~seen~~  
286 in simulations (Saenko et al., 2004; Chikamoto et al., 2012; Hu et al., 2012) as well as in

287 ~~observations~~ reconstructions (Okazaki et al., 2010; Menviel et al., 2014; Freeman et al., 2015)  
288 ~~based on~~ for the last deglaciation. Such studies have also suggested that large PMOC–AMOC  
289 seesaw modulations can be triggered by slight changes in the freshwater/salinity redistributions  
290 between the Pacific and Atlantic. Furthermore, we provide an insight that the maintenance  
291 mechanism of PMOC in without the TP, to some extent, is the same as the AMOC in the present  
292 day. Specially, for the current North Atlantic, there is a persistently northward movement of warm  
293 and salty water mass from the tropical-subtropical Gulf Stream region into North Atlantic and  
294 farther poleward into the Norwegian and Greenland Seas, where it is exposed to very cold  
295 atmospheric temperatures and followed by a gradual cooling and in turn a higher density due to  
296 the release substantial sensible and latent heat into the overlying cold atmosphere, which is the  
297 same as PMOC, before eventually forming the North Atlantic Deep Water.

298 Our simulations have potential implications for understanding paleotemperature  
299 reconstructions and paleoceanographic circulation reorganization. The Earth has experienced a  
300 long-term cooling trend throughout the Cenozoic ~~on the basis of~~ as testified by many proxies and  
301 stacked records (Zachos et al., 2001, 2008), in association with an ~~reduced~~ increased  
302 ~~equator-to-pole~~ equator-to-pole thermal gradient. A very important contribution to understanding  
303 the large cooling during the Cenozoic has been determined as the drastic decrease in atmospheric  
304 CO<sub>2</sub> since the Eocene (DeConto and Pollard, 2003; DeConto et al., 2008). On the other hand, a  
305 study with new data base further indicated that this thermal evolution has been different among  
306 ocean basins during the Cenozoic (Cramer et al., 2009), and this differing evolutionary pattern  
307 between basins is largely related to the large-scale ocean dynamics and tectonic events (Zhang et  
308 al., 2011). Moreover, epsilon-Neodymium (eps-Nd) isotopes in the deep Pacific suggest that the  
309 North Pacific was characterized by vigorous deep water formation during ca. 65–40 Ma (Thomas,

310 2004). Other new eps-Nd records also confirm that the overturning circulation was already  
311 established in the high-latitude North Pacific prior to 40 Ma (Hague et al., 2012; Thomas et al.,  
312 2014). In comparison, a modern-like bipolar oceanic circulation, characterized by two branches of  
313 deep water formation in the ~~S~~southern ~~O~~cean and ~~the~~ North Atlantic, began in the late Eocene  
314 (~38.5 Ma) in relation to the effect of ~~southern-Southern ocean-Ocean~~ gateway openings (Borrelli  
315 et al., 2014). Several records also support that the onset of the present AMOC state began at the  
316 Eocene–Oligocene transition (~34 Ma) in association with the tectonic deepening of the  
317 Greenland–Norwegian Sea (Wright and Miller, 1993; Davies et al., 2001; Via and Thomas, 2006).  
318 However, it is likely that the intermittent Cenozoic uplift of the TP reached a certain height by the  
319 Early Oligocene, as shown in geologic evidences (Dupont-Nivet et al., 2008; Wang et al., 2008).  
320 Our own contribution demonstrates that ~~the~~ major uplift occurring during this period was also an  
321 important player in climate changes via hydrologic and ocean dynamics changes. Indeed, we  
322 pinpoint the drastic effect of TP uplift alone on the distribution of the northern hemispheric MOCs  
323 and potentially provide clues for proxy record interpretation.

324 Finally, this simulation is performed with ~~the~~ constant atmospheric CO<sub>2</sub> concentrations at the  
325 pre-industrial, whereas it was higher during the uplift phase in the real world. In the context of  
326 past warm world, such as Late Eocene, the climate conditions are accompanied ~~with-by~~ high  
327 atmospheric CO<sub>2</sub> concentration, limited sea ice extent, and significantly modified land–sea  
328 distribution. Under these warmer boundary conditions, the responses of AMOC to the TP induced  
329 freshwater forcing may be very different from the modern conditions (~~e.g., Vavrus and Kutzbach,~~  
330 ~~2002~~). Therefore, it will be necessary to perform further numerical experiments with more  
331 realistic boundary conditions to accurately investigate the contribution of the TP uplift on ~~the~~  
332 oceanic circulation and therefore to be able to compare with data reconstructions.

333 *Acknowledgements* We sincerely thank the two anonymous reviewers for their insightful  
334 comments and suggestions to improve this manuscript. We also thank Dr. Jiang Zhu for  
335 discussions and technical support during the writing of the paper. This work was supported by the  
336 National Natural Science Foundation of China (41421004, 41572159, and 41625018).

337 Reference

- 338 Abe, M., Kitoh, A., and Yasunari, T.: An evolution of the Asian summer monsoon associated with mountain  
339 uplift—simulation with the MRI atmosphere-ocean coupled GCM, *J. Meteorol. Soc. Jpn.*, 81, 909–933,  
340 2003.
- 341 An, Z., Kutzbach, J. E., Prell, W. L., and Porter, S. C.: Evolution of Asian monsoons and phased uplift of the  
342 Himalaya–Tibetan plateau since Late Miocene times, *Nature*, 411, 62–66, 2001.
- 343 Bolin, B.: On the influence of the earth's orography on the general character of the westerlies, *Tellus*, 2,  
344 184–195, 1950.
- 345 Borrelli, C., Cramer, B. S., and Katz, M. E.: Bipolar Atlantic deepwater circulation in the middle-late Eocene:  
346 Effects of southern ocean gateway openings, *Paleoceanography*, 29, 308–327, 2014.
- 347 [Botsyun, S., Sepulchre, P., Risi, C., Donnadieu, Y.: Impacts of Tibetan Plateau uplift on atmospheric dynamics  
348 and associated precipitation  \$\delta^{18}\text{O}\$ , \*Clim. Past\*, 12, 1401–1420, 2016.](#)
- 349 Broccoli, A. J., and Manabe, S.: The effects of orography on midlatitude northern hemisphere dry climates, *J.*  
350 *Clim.*, 5, 1181–1201, 1992.
- 351 Chikamoto, M. O., Menviel, L., Abe-Ouchi, A., Ohgaito, R., Timmermann, A., Okazaki, Y., Harada, N., Oka, A.,  
352 and Mouchet, A.: Variability in North Pacific intermediate and deep water ventilation during Heinrich  
353 events in two coupled climate models, *Deep-Sea Res. PT. II*, 61–64, 114–126, 2012.
- 354 Cramer, B. S., Toggweiler, J. R., Wright, J. D., Katz, M. E., and Miller, K. G.: Ocean overturning since the Late  
355 Cretaceous: Inferences from a new benthic foraminiferal isotope compilation, *Paleoceanography*, 24,  
356 PA4216, doi:10.1029/2008PA001683, 2009.
- 357 Cunningham, S. A., Kanzow, T., Rayner, D., Baringer, M. O., Johns, W. E., Marotzke, J., Longworth, H. R.,  
358 Grant, E. M., Hirschi, J. J.-M., Beal, L. M., Meinen, C. S., and Bryden, H. L.: Temporal variability of the  
359 Atlantic meridional overturning circulation at 26.5°N, *Science*, 317, 935–938,  
360 doi:10.1126/science.1141304, 2007.
- 361 Davies, R., Cartwright, J., Pike, J., and Line, C.: Early Oligocene initiation of North Atlantic deep water  
362 formation, *Nature*, 410, 917–920, 2001.
- 363 DeConto, R. M., and Pollard, D.: Rapid Cenozoic glaciation of Antarctica induced by declining atmospheric

364 CO<sub>2</sub>, *Nature*, 421, 245–249, 2003.

365 DeConto, R. M., Pollard, D., Wilson, P. A., Pälike, H., Lear, C., and Pagani, M.: Thresholds for Cenozoic  
366 bipolar glaciation, *Nature*, 455, 652–657, 2008.

367 Dupont-Nivet, G., Hoorn, C., and Konert, M.: Tibetan uplift prior to the Eocene-Oligocene climate transition:  
368 Evidence from pollen analysis of the Xining Basin, *Geology*, 36, 987–990, 2008.

369 Emile-Geay, J., Cane, M. A., Naik, N., Seager, R., Clement, A. C., and van Geen, A.: Warren revisited:  
370 Atmospheric freshwater fluxes and “Why is no deep water formed in the North Pacific”, *J. Geophys.*  
371 *Res.*, 108(C6), 3178, doi:10.1029/2001JC001058, 2003.

372 Fallah, B., Cubasch, U., Prömmel, K., and Sodoudi, S.: A numerical model study on the behaviour of Asian  
373 summer monsoon and AMOC due to orographic forcing of Tibetan Plateau, *Clim. Dyn.*, 47, 1485–1495,  
374 2016.

375 Feng, R., and Poulsen, C. J.: Andean elevation control on tropical Pacific climate and ENSO, *Paleoceanography*,  
376 29, 795–809, 2014.

377 Freeman, E., Skinner, L. C., Tisserand, A., Dokken, T., Timmermann, A., Menviel, L., and Friedrich, T.: An  
378 Atlantic–Pacific ventilation seesaw across the last deglaciation, *Earth Planet. Sci. Lett.*, 424, 237–244,  
379 2015.

380 Gent, P. R., Danabasoglu, G., Donner, L. J., Holland, M. M., Hunke, E. C., Jayne, S. R., Lawrence, D. M.,  
381 Neale, R. B., Rasch, P. J., Vertenstein, M., Worley, P. H., Yang, Z. L., and Zhang, M.: The Community  
382 Climate System Model version 4, *J. Clim.*, 24, 4973–4991, doi:10.1175/2011JCLI4083.1, 2011.

383 Hague, A. M., Thomas, D. J., Huber, M., Korty, R., Woodard, S. C., and Jones, B. L.: Convection of North  
384 Pacific deep water during the early Cenozoic, *Geology*, 40, 527–530, 2012.

385 Holland, M. M., Bailey, D. A., Briegleb, B. P., Light, B., and Hunke, E.: Improved sea ice shortwave radiation  
386 physics in CCSM4: The impact of melt ponds and black carbon, *J. Clim.*, 25, 1413–1430, 2012.

387 Hu, A., Meehl, G. A., Han, W., Timmermann, A., Otto-Bliesner, B., Liu, Z., Washington, W. M., Large, W.,  
388 Abe-Ouchi, A., Kimoto, M.: Role of the Bering Strait on the hysteresis of the ocean conveyor belt  
389 circulation and glacial climate stability, *Proc. Natl. Acad. Sci. U. S. A.*, 109, 6417–6422, 2012.

390 Jayne, S. R., and Marotzke, J.: A destabilizing thermohaline circulation–atmosphere–sea ice feedback, *J. Clim.*,

391 12, 642–651, 1999.

392 Jiang, D., Ding, Z. L., Drange, H., and Gao, Y.: Sensitivity of East Asian climate to the progressive uplift and  
393 expansion of the Tibetan Plateau under the mid-Pliocene boundary conditions, *Adv. Atmos. Sci.*, 25,  
394 709–722, 2008.

395 Kitoh, A.: Effects of mountain uplift on East Asian summer climate investigated by a coupled  
396 atmosphere–ocean GCM, *J. Clim.*, 17, 783–802, 2004.

397 ~~Kitoh, A., Motoi, T., Arakawa, Q.: Climate modeling study on mountain uplift and Asian monsoon evolution,~~  
398 ~~*Geol. Soc. Lond. Spec. Publ.*, 342, 293–301, doi:10.1144/SP342.17, 2010~~

399 Kutzbach, J. E., Prell, W. L., and Ruddiman, W. F.: Sensitivity of Eurasian climate to surface uplift of the  
400 Tibetan Plateau, *J. Geol.*, 101, 177–190, 1993.

401 Liu, X., and Yin, Z.-Y.: Sensitivity of East Asian monsoon climate to the uplift of the Tibetan Plateau,  
402 *Palaeogeogr. Palaeoclim. Palaeoecol.*, 183, 223–245, 2002.

403 Maffre, P., Ladant, J. B., Donnadieu, Y., Sepulchre, P., and Godd ris, Y.: The influence of orography on modern  
404 ocean circulation, *Clim. Dyn.*, doi:10.1007/s00382-017-3683-0, 2017.

405 Menviel, L., England, M. H., Meissner, K. J., Mouchet, A., and Yu, J.: Atlantic-Pacific seesaw and its role in  
406 outgassing CO<sub>2</sub> during Heinrich events, *Paleoceanography*, 29, 58–70, 2014.

407 Molnar, P., Boos, W. R., and Battisti, D. S.: Orographic controls on climate and paleoclimate of Asia: Thermal  
408 and mechanical roles for the Tibetan Plateau, *Annu. Rev. Earth. Planet. Sci.*, 38, 77–102, 2010.

409 Nilsson, J., Langen, P., Ferreira, D., and Marshall, J.: Ocean basin geometry and the salinification of the Atlantic  
410 Ocean, *J. Clim.*, 26, 6163–6184, 2013.

411 Okajima, H., and Xie, S. P.: Orographic effects on the northwestern Pacific monsoon: Role of air-sea interaction,  
412 *Geophys. Res. Lett.*, 34, L21708, doi: 10.1029/2007GL032206, 2007.

413 Okazaki, Y., ~~A.~~ Timmermann, ~~A.~~ Menviel, L., Harada, N., Abe-Ouchi, A., Chikamoto, M. O., Mouchet, A., and  
414 Asahi, H.: Deepwater formation in the North Pacific during the last glacial termination, *Science*, 329,  
415 200–204, 2010.

416 Palmer, T. N., Shutts, G. J., and Swinbank, R.: Alleviation of a systematic westerly bias in general circulation

417 and numerical weather prediction models through an orographic gravity wave drag parametrization, *Q. J.*  
418 *R. Meteorol. Soc.*, 112, 1001–1039, 1986.

419 Ramstein, G., Fluteau, F., Besse, J., and Jousaume, S.: Effect of orogeny, plate motion and land-sea distribution  
420 on Eurasian climate change over the past 30 million years, *Nature*, 386, 788–795, 1997.

421 Rind, D., Russell, G., and Ruddiman, W. F.: The effects of uplift on Ocean–Atmosphere, in: *Tectonic Uplift and*  
422 *Climate Change*, Ruddiman, W. F. (Ed.), Plenum Press, New York, 123–147, 1997.

423 Rodwell, M. J., and Hoskins, B. J.: Subtropical anticyclones and summer monsoons, *J. Clim.*, 14, 3192–3211,  
424 2001.

425 Ruddiman, W. F., and Kutzbach, J. E.: Forcing of Late Cenozoic northern hemisphere climate by plateau uplift  
426 in southern Asia and the American West, *J. Geophys. Res.*, 94(D15), 18409–18427, 1989.

427 Saenko, O. A., Schmittner, A., and Weaver, A. J.: The Atlantic-Pacific seesaw, *J. Clim.*, 17, 2033–2038, 2004.

428 Schmitt, R. W., Bogden, P. S., and Dorman, C. E.: Evaporation minus precipitation and density fluxes for the  
429 North Atlantic, *J. Phys. Oceanogr.*, 19, 1208–1221, 1989.

430 Schmittner, A., Silva, T. A. M., Fraedrich, K., Kirk, E., and Lunkeit, F.: Effects of mountains and ice sheets on  
431 global ocean circulation, *J. Clim.*, 24, 2814–2829, 2011.

432 Seager, R., Battisti, D. S., Yin, J., Gordon, N., Naik, N., Clement, A. C., and Cane, M. A.: Is the Gulf Stream  
433 responsible for Europe's mild winters?, *Q. J. R. Meteorol. Soc.*, 128, 2563–2586, 2002.

434 Sepulchre, P., Sloan, L. C., Snyder, M., and Fiechter, J.: Impacts of Andean uplift on the Humboldt Current  
435 system: A climate model sensitivity study, *Paleoceanography*, 24, PA4215, doi:10.1029/2008PA001668,  
436 2009.

437 | Shields, C. A., Bailey, D. A., Danabasoglu, G., Jochum, M., Kiehl, J. T., Levis, S., and Park, S.: The  
438 low-resolution CCSM4, *J. Clim.*, 25, 3993–4014, 2012.

439 Sinha, B., Blaker, A. T., Hirschi, J., Bonham, S., Brand, M., Josey, S., Smith, R. S., and Marotzke, J.: Mountain  
440 ranges favour vigorous Atlantic meridional overturning, *Geophys. Res. Lett.*, 39, L02705,  
441 doi:10.1029/2011GL050485, 2012.

442 Spence, J., Eby, M., and Weaver, A.: The sensitivity of the Atlantic meridional overturning circulation to

443 freshwater forcing at eddy-permitting resolutions, *J. Clim.*, 21, 2697–2710, 2008.

444 Thomas, D. J.: Evidence for deep-water production in the North Pacific Ocean during the early Cenozoic warm  
445 interval, *Nature*, 430, 65–68, 2004.

446 Thomas, D. J., Korty, R., Huber, M., Schubert, J. A., and Haines, B.: Nd isotopic structure of the Pacific Ocean  
447 70–30 Ma and numerical evidence for vigorous ocean circulation and ocean heat transport in a  
448 greenhouse world, *Paleoceanography*, 29, 454–469, 2014.

449 [Vavrus, S., and Kutzbach, J. E.: Sensitivity of the thermohaline circulation to increased CO<sub>2</sub> and lowered  
450 topography, \*Geophys. Res. Lett.\*, 29, 1546, doi:10.1029/2002GL014814, 2002.](#)

451 Via, R. K., and Thomas, D. J.: Evolution of Atlantic thermohaline circulation: Early Oligocene onset of  
452 deep-water production in the North Atlantic, *Geology*, 34, 441–444, 2006.

453 Wang, C., Zhao, X., Liu, Z., Lippert, P. C., Graham, S. A., Coe, R. S., Yi, H., Zhu, L., Liu, S., and Li, Y.:  
454 Constraints on the early uplift history of the Tibetan Plateau, *Proc. Natl. Acad. Sci. U. S. A.*, 105,  
455 4987–4992, 2008.

456 Warren, B. A.: Why is no deep water formed in the North Pacific?, *J. Mar. Res.*, 41, 327–347, 1983.

457 Weaver, A. J., Bitz, C. M., Fanning, A. F., and Holland, M. M.: Thermohaline circulation: High-latitude  
458 phenomena and the difference between the Pacific and Atlantic, *Annu. Rev. Earth. Planet. Sci.*, 27,  
459 231–285, 1999.

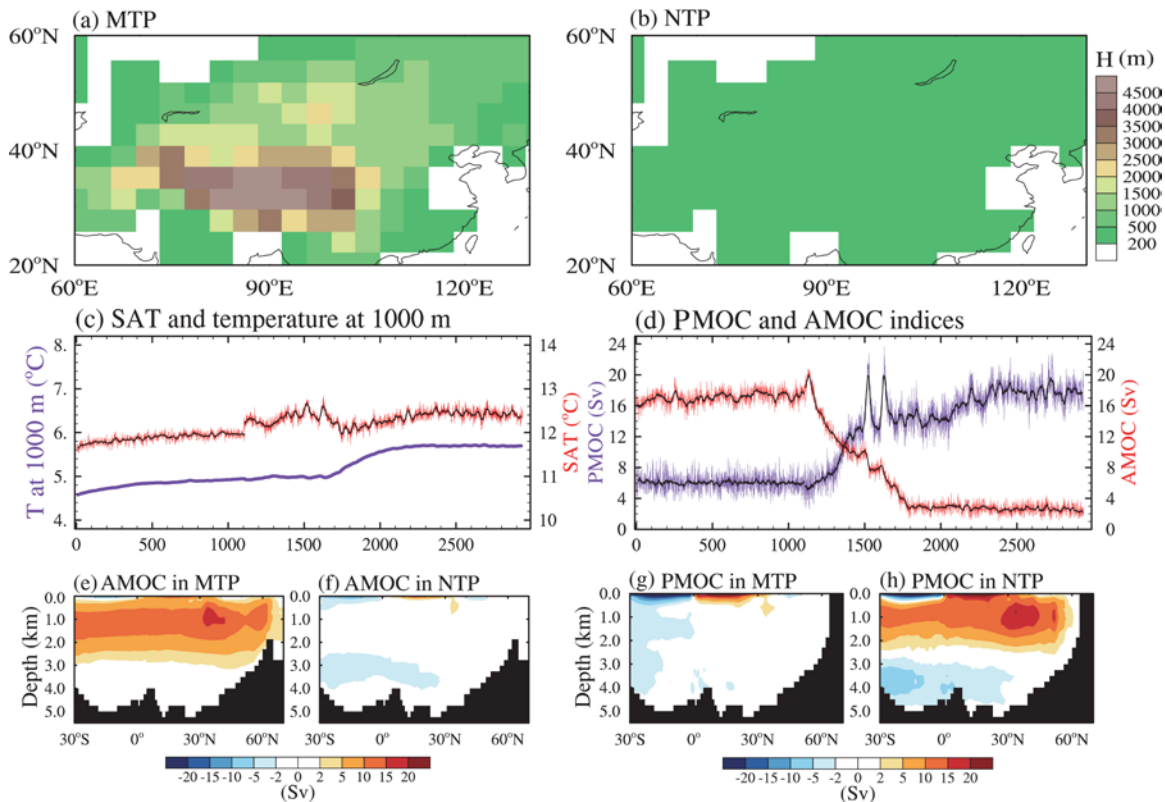
460 Wright, J. D., and Miller, K. G.: Southern ocean influences on late Eocene to Miocene deepwater circulation, in:  
461 The Antarctic Paleoenvironment: A perspective on global change part two, Kennett, J. P. and Warnke, D.  
462 A. (Eds.), American Geophysical Union, Washington, 1–25, 1993.

463 Zachos, J., Pagani, M., Sloan, L., Thomas, E., and Billups, K.: Trends, rhythms, and aberrations in global  
464 climate 65 Ma to present, *Science*, 292, 686–693, 2001.

465 Zachos, J. C., Dickens, G. R., and Zeebe, R. E.: An early Cenozoic perspective on greenhouse warming and  
466 carbon-cycle dynamics, *Nature*, 451, 279–283, 2008.

467 Zhang, R., Jiang, D., Zhang, Z., and Yu, E.: The impact of regional uplift of the Tibetan Plateau on the Asian  
468 monsoon climate, *Palaeogeogr. Palaeoclim. Palaeoecol.*, 417, 137–150, 2015.

- 469 Zhang, Z., Nisancioglu, K. H., Flatoy, F., Bentesen, M., Bethke, I., and Wang, H.: Tropical seaways played a  
470 more important role than high latitude seaways in Cenozoic cooling, *Clim. Past*, 7, 801–813, 2011.
- 471 Zhu, J., Liu, Z., Zhang, X., Eisenman, I., and Liu, W.: Linear weakening of the AMOC in response to receding  
472 glacial ice sheets in CCSM3, *Geophys. Res. Lett.*, 41, 6252–6258, 2014.



473

474 **Figure 1.** Two topographic height configurations used in experiments: (a) MTP and (b) NTP. (c)

475 Time series of global mean annual 2-m surface air temperature (SAT) and sea temperature at 1000

476 m depth in MTP (1–1100 years) and NTP (1101–2940 years) simulations; bold black lines show

477 21-year running mean. (d) Same as (c) but for PMOC and AMOC indices, respectively. AMOC

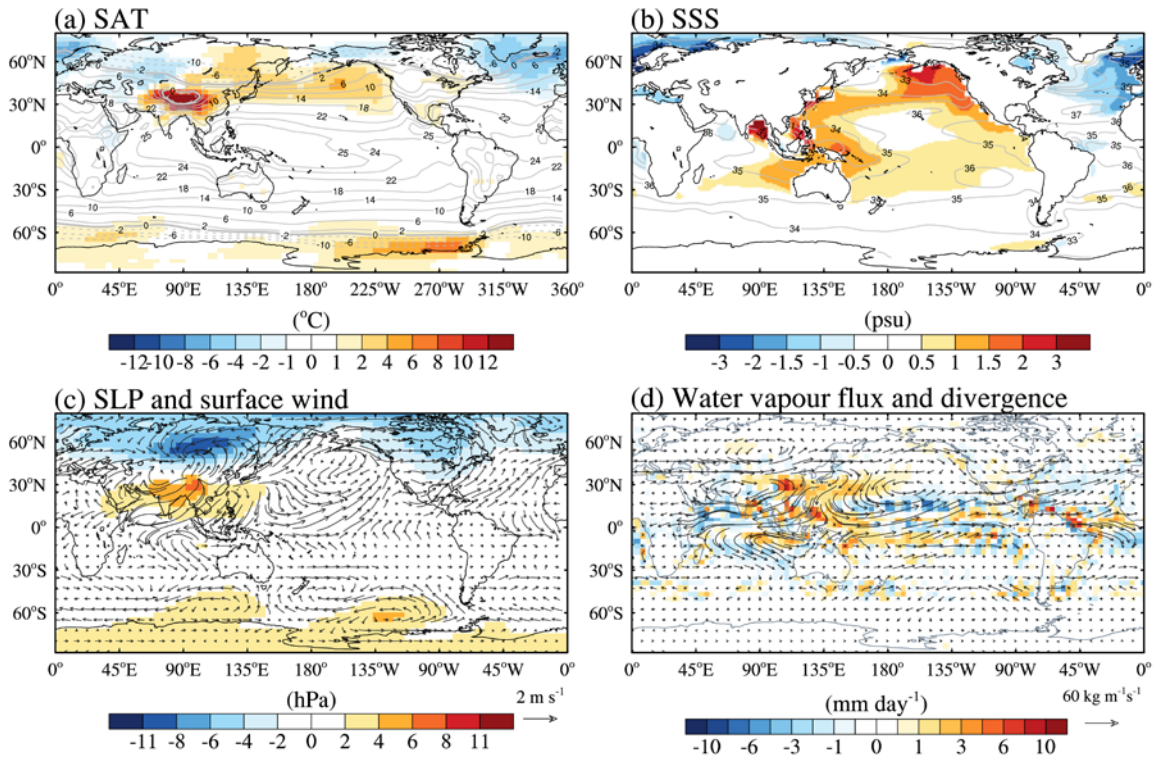
478 and PMOC indices are defined as the annual maximum of the meridional stream function value

479 north of 28°N and below the depth of 500 m over the North Atlantic and Pacific, respectively.

480 (e–h) Climatological annual mean Atlantic and Indian–Pacific meridional overturning stream

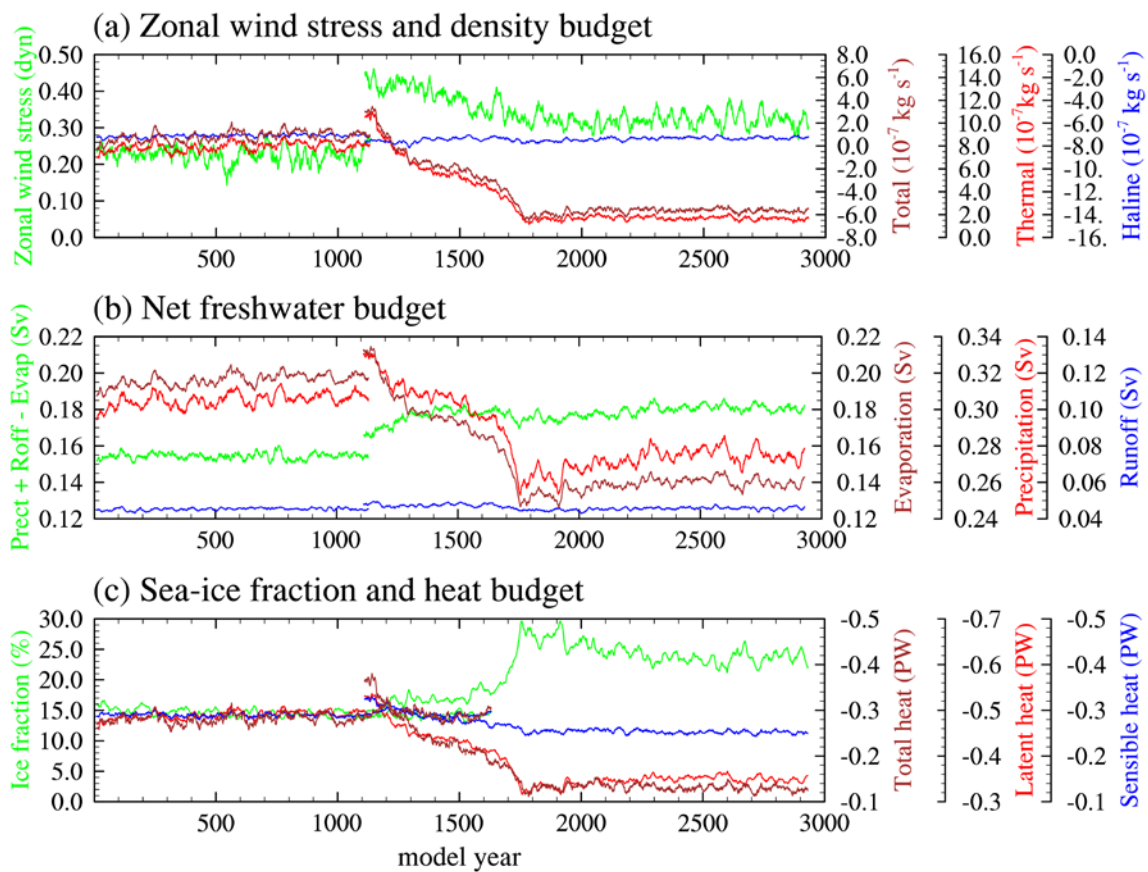
481 function in MTP (e and g) and NTP (f and h); positive (negative) shading represents clockwise

482 (counterclockwise) circulations.



483

484 **Figure 2.** (a) Climatological SAT in MTP (contour) and anomalies (shaded) for NTP minus MTP;  
 485 (b) same as Figure 2a, but for sea surface salinity (SSS); (c) changes in sea-level pressure (SLP,  
 486 shading) and surface wind (vectors); and (d) vertically integrated (surface to 300 hPa pressure  
 487 layer) water vapor flux (vectors) and its convergence (shading) in NTP relative to MTP. Unit of  
 488 convergence is converted to  $\text{mm day}^{-1}$  assuming the density of liquid water as  $1 \text{ g cm}^{-3}$ .



489

490 **Figure 3.** Regional annual mean across North Atlantic basin at 40°–70°N for MTP (1–1100 years)

491 and NTP (1101–2940 years) of (a) zonal surface wind-stress, total density flux, haline density flux,

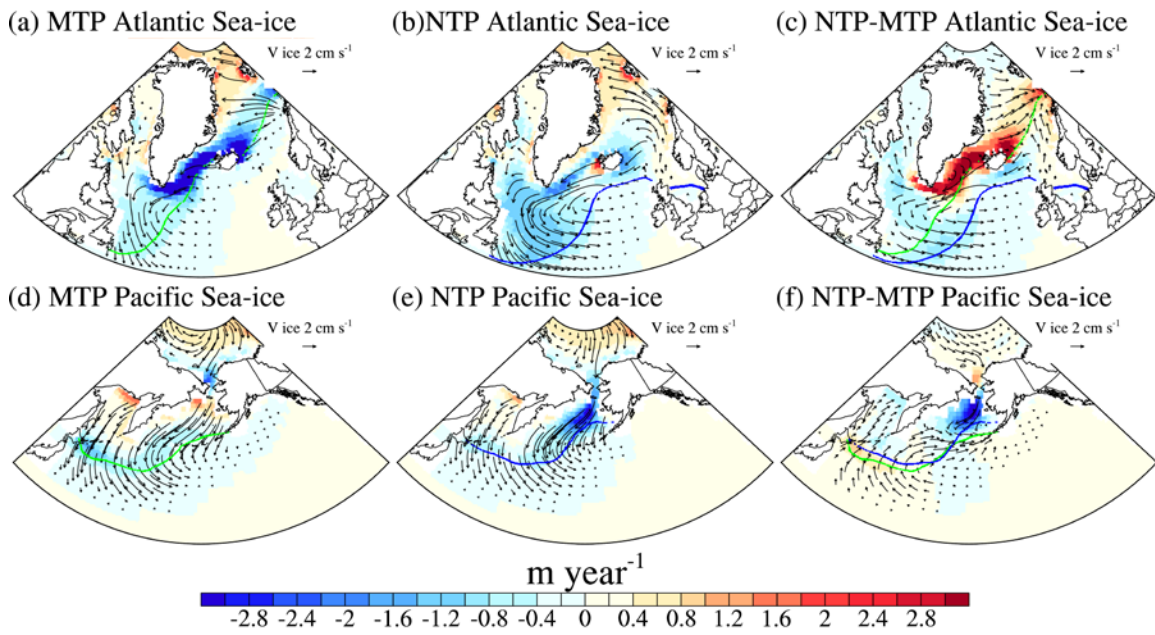
492 and thermal density flux (total density flux is decomposed into haline contribution due to

493 freshwater flux and thermal contribution due to heat flux (*Schmitt et al.*, 1989); (b) net freshwater,

494 precipitation, runoff, and evaporation fluxes; (c) sea-ice fraction, total heat, sensible heat, and

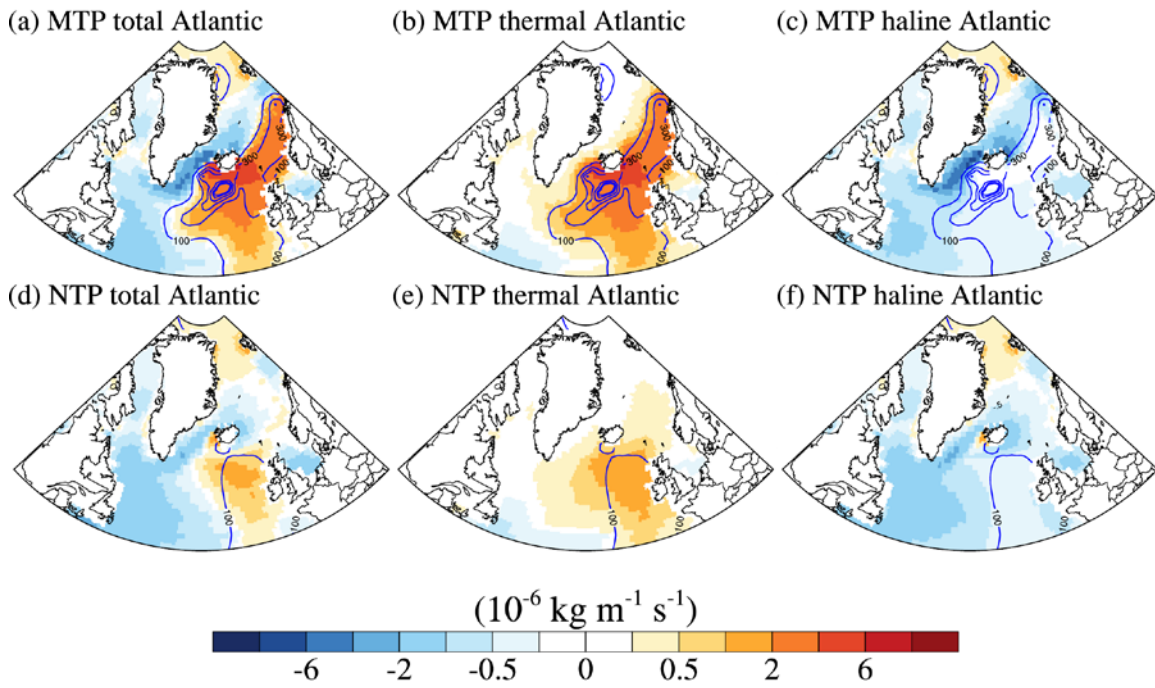
495 latent heat fluxes, (units: PW, 1 PW =  $10^{15}$  W). For comparison purposes, all lines with common

496 units use identical vertical scale spacing.



497

498 **Figure 4.** The North Atlantic and Pacific region features of annual mean sea-ice formation rate  
 499 (shading; positive stands for formation, and negative stands for melting), sea-ice velocity (vectors,  
 500  $\text{cm s}^{-1}$ ), and for (a, d) MTP, (b, e) NTP, and (c, f) difference between NTP and MTP. The February  
 501 sea-ice margin is indicated with dashed lines (defined as the 15% sea-ice coverage, green line for  
 502 MTP, blue line for NTP)



503

504

505

506

507

**Figure 5.** The North Atlantic annual mean (a, d) total density flux (shading; positive means flux makes water denser), (b, e) the thermal density flux, (c, f) the haline density flux, and the winter mixed layer depth (blue contour, contour interval: 200 m) in the MTP (upper panel) and NTP (lower panel).

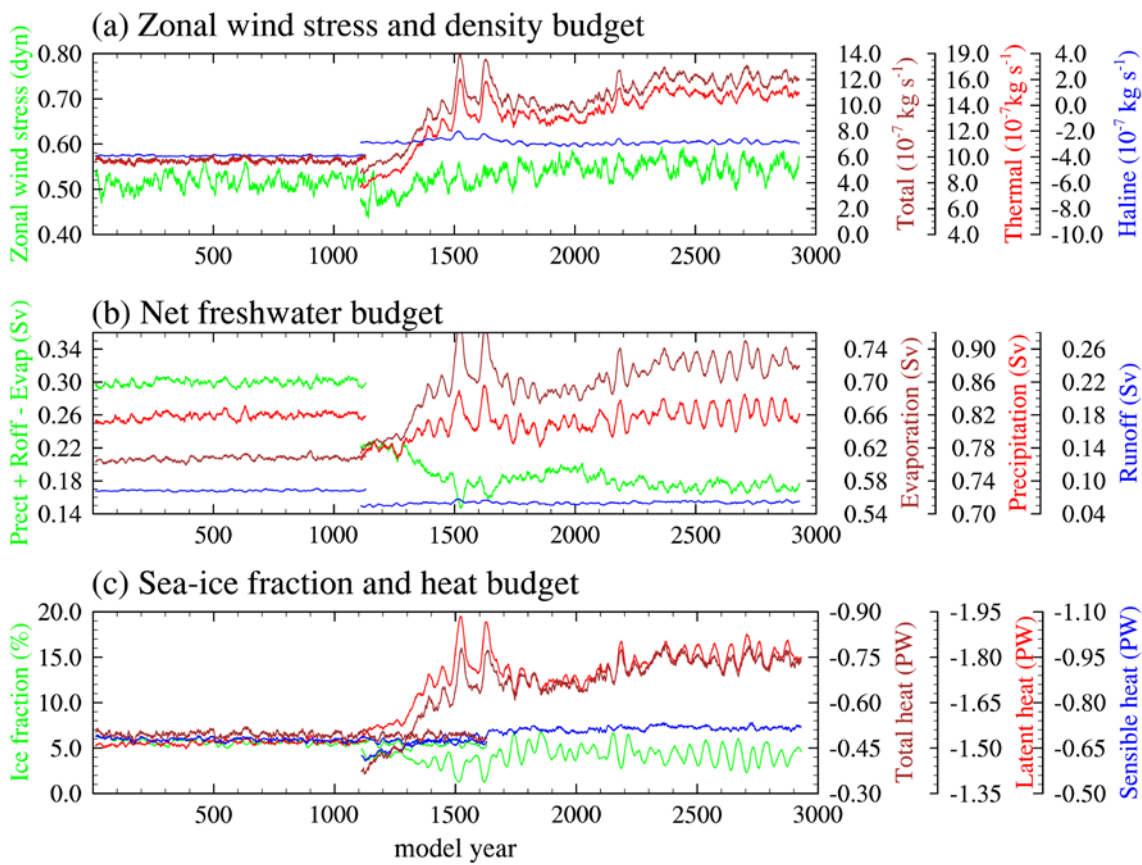
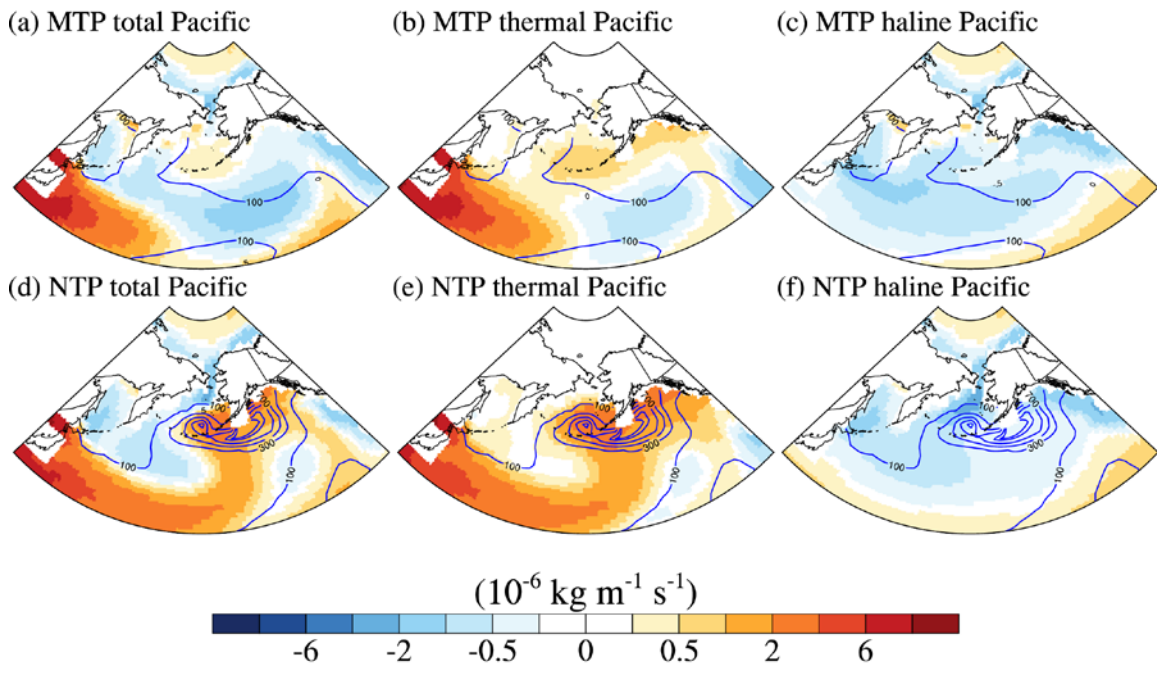
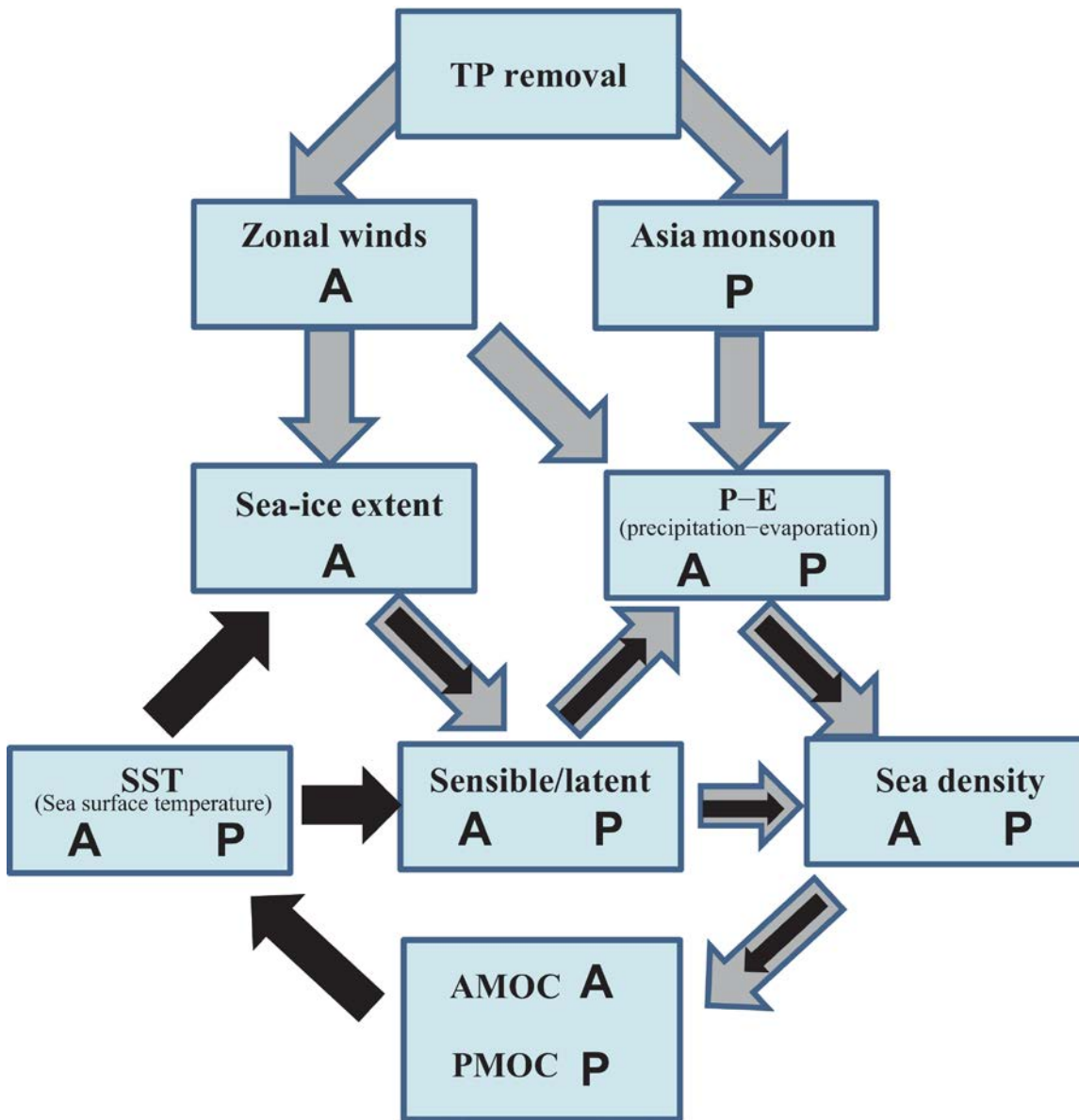


**Figure 6.** As in Figure 3, but for North Pacific basin at 30°–70°N.



510

511 **Figure 7.** The same as Figure 5, but for the North Pacific (30–80°N).



512

513 **Figure 8.** Schematic diagram about the influence of the removal of TP on the AMOC and PMOC.

514 Vectors in gray denote the climate responses in relation to the increased in wind-induced and

515 decreased monsoonal-driven net precipitation-evaporation and wind-driven sea-ice processes. The

516 black color vectors denote the feedback processes ~~related to the AMOC weakening~~.

517 characters A and P stand for the physical processes occurring over the North Atlantic and Pacific,

518 respectively.